Aquaporin-based membranes made by interfacial polymerization in hollow fibers: visualization and role of aquaporin in water permeability.

Running Title: Aquaporin Z requirement in hollow fibers

Loveena Sharma[1,2], Li Ye[2,3], Clare Yong[1], Ramya Seetharaman[1,2], Kailing Kho[1,2], Wahyu Surya[1], Wang Rong[2,3] and Jaume Torres[1,2,#]

[1]School of Biological Sciences, Nanyang Technological University, 637551, Singapore.
[2]Singapore Membrane Technology Centre, Nanyang Environment and Water Research Institute, Nanyang Technological University, 639798, Singapore.
[3]School of Civil and Environmental Engineering, Nanyang Technological University, 639798, Singapore.

[#]To whom correspondence should be addressed: Jaume Torres; School of Biological Sciences, Nanyang Technological University, 60 Nanyang Drive, 637551 Singapore; Tel: +65 6316 2857; Fax: +65 6791 3856; E-mail: jtorres@ntu.edu.sg

ABSTRACT

Aquaporins are water channel proteins with high permeability and solute rejection, making them ideal components for the preparation of desalination biomimetic membranes. In one strategy, *E. coli* aquaporin Z (AqpZ) proteoliposomes are immobilized in a polyamide layer formed by interfacial polymerization at the inner surface of hollow fibers. However, once polymerization occurs, the system is almost a black box where it is difficult to disentangle the relative contribution to performance of (i) water permeation through AqpZ channels and (ii) the possible modification of the properties or structure of the polymer layer by the mere presence of protein and lipid. Indeed, the fate of protein and lipid once the polymer is formed, and how much of it is actually used, is under debate. Also, the performance of these modules has been reported to be stable over several months. This is intriguing because of the expected degradation of functional AqpZ and lipid with time. Herein, we used lipid and AqpZ, both fluorescently labeled, to unequivocally localize both components only at the inner surface of the hollow fibers. To characterize module performance, we tested about 30 half-inch modules containing five hollow fibers each. Those reconstituted with wild type AqpZ produced higher permeability (~8.5 ± 0.9 LMH/bar) than those reconstituted with AqpZ mutant (R189A) (~5.6 ± 1.7 LMH/bar) or lipid-only liposomes (3.7 ± 1.1 LMH/bar). However, while these differences are significant, they are smaller than expected from the comparison of relative permeabilities of membranes incorporating wild-type AqpZ, R189A mutant and only-lipid. In addition, we show that in a five-month long experiment, performance of two of these modules showed only minor deterioration, if any, which is not consistent with the observed rapid degradation of proteoliposomes at room temperature. Overall, these data obtained in this set-up suggests that although both AqpZ and lipid are localized at the inner of the hollow fibers, they mainly behave as additives that modify the properties of the robust polyamide layer. A small contribution of AqpZ channel activity to module performance is possible, but to be significant it would require full coverage and a higher protein density in the proteoliposomes, which at present cannot be achieved in the current protocol.

Keywords – Aquaporin Z, fluorescent dyes, hollow fibers, confocal microscopy, interfacial polymerization

1. Introduction

Due to the growing demand for safe fresh water, one of the multiple applications of selective membranes is water reuse and desalination. Reverse osmosis (RO) and thin-film composite (TFC) membranes provide high-quality water by removing almost all impurities including ions and small organic molecules [1]. A variety of synthetic channels have been inspired by biological water channels for incorporation into TFC membranes [2]. However, direct incorporation of natural biological channels such as aquaporins (AQPs) into synthetic environments is also possible. AQPs permeabilize membranes to water and other small solutes [3-5]. They have a tetrameric architecture that is very conserved from bacteria to humans [6-12], where each monomer functions as a water channel [13] subject to a degree of cooperativity [14]. Orthodox aquaporins like *E. coli* aquaporin Z (AqpZ) reject other solutes, including protons, and can deliver a water flux of up to ~3 billion water molecules per second [15, 16].

Aquaporin-based biomimetic membranes (ABMs) have attracted considerable interest over the last decade. In one successful design, AqpZ proteoliposomes in a solution of m-phenylenediamine (MPD) are used to soak the inner surface of an ultrafiltration (UF) hollow fiber membrane. After the addition of trimesoyl chloride (TMC), a polyamide layer is formed by interfacial polymerization (IP). In a hypothetical 'encased' model [17], formation of this IP layer constitutes a protective environment for the incorporated AqpZ proteoliposomes, which is critical for retaining activity over long term operation in practical applications. Compared with commercial RO membranes, ABMs require half of the applied pressure to achieve the same water flux, therefore they can potentially reduce energy consumption [18]. This design can be easily scaled up and may lead to the design and development of a new generation of AQP-based hollow fiber membranes for RO and forward osmosis (FO) applications.

However, it is difficult to visualize AqpZ proteoliposomes trapped or embedded within the crosslinked polyamide matrix that covers the inner face of these porous hollow fibers [18-20]. Electron microscopy images show a few intact liposomes [18, 21, 22], but whether other liposomes form a homogeneous layer or are trapped in an intact form in the ~ 300 nm thick IP skin is not known. It is also not known if these liposomes are only localized only at the inner surface of these hollow fibers, or if they are also found inside the walls and the outer surface. The presence of AqpZ and lipid in the polyamide layer has been inferred indirectly from carbon, oxygen and nitrogen ratios, or from phosphorous quantification of lipid [22]. Finally, it is intriguing that these modules can

allegedly perform for several months [23], therefore the presence of lipid and AqpZ in the IP layer, and their precise role in the performance of these modules has been under debate.

To visualize the localization of AqpZ and lipid fractions in the hollow fibers after IP layer formation, we have used confocal microscopy after incorporation of fluorescently labeled AqpZ and lipid. While labeled lipids are commercially available, AqpZ was chemically labeled in-house. A small dye was preferred, since using a bulky fusion protein like green fluorescent protein (GFP) may have altered the behavior of proteoliposomes in solution and in the IP layer.

Lastly, since the performance of these modules showed large variability, statistically significant results to investigate the role of AqpZ and lipid in water permeability could only be obtained after comparing about 30 half-inch modules containing five hollow fibers each. Overall, our results provide a critical assessment of the relative importance of the water channel activity of AqpZ in these hollow fibers, suggesting that it is the modification of the polyamide layer properties that is a critical factor in module performance.

2. MATERIALS AND METHODS.

2.1 *Aquaporin Z proteoliposome preparation*.

Aquaporin Z (AqpZ) in 3% octyl-β-D-glucoside (OG) was obtained from ion-exchange and affinity chromatography using methods described previously [18]. *E. coli* total lipid (ECL, 100500P) was obtained from Avanti® Polar Lipids, Inc (Alabama, US) in powder form. The lipid powder was solubilized in chloroform (100 mg/mL) and stored at -20 °C in glass vials. Liposomes were prepared using the film rehydration method [24]. The chloroform was evaporated under a nitrogen gas stream and the dry lipid film was exposed to vacuum overnight at 4 °C in the dark. The vacuum was filled with Argon gas before retrieving the vials. The film was rehydrated (Fig. 1A, step 1) by addition of stock AqpZ to achieve a molar lipid-to-protein ratio (mLPR) of 400:1, where protein refers to monomeric AqpZ (mAqpZ). Stock AqpZ in OG was diluted typically ~ 10x in phosphate buffer saline (PBS). Final nominal concentration of AqpZ, lipid and OG was 0.6 mg/mL (24 μM), 8 mg/mL (10 mM) and 0.3%, respectively, with Osm_{PBS} ~ 295-299 mmol/Kg. The mixture was vortexed vigorously, freeze-thawed three times with liquid nitrogen and warm water (44 °C), and incubated for 1 h at room temperature (Fig. 1A, step 2). Liposomes of uniform size distribution were prepared by extrusion through sequential passage first through 400 nm and later 200 nm pore-size polycarbonate membranes using an Avestin extruder (Avestin Inc., Ottawa, Canada) (Fig. 1A, step 3). The process typically resulted in liposomes of 150-200 nm in diameter and PDI < 0.2. To obtain lipid-only liposomes, i.e., without AqpZ, the procedure was the same,

except that the buffer added to the dry lipids did not contain AqpZ or OG. Proteoliposomes were stored at 4 °C and used on the same day. Samples used in stopped flow measurements and during soaking of the hollow fibers where further diluted 10x, i.e., they contained a final OG of 0.03%, far below the OG cmc (~0.75%).

2.2. Determination of OG concentration.

OG concentration was measured using a colorimetric glucoside assay [25, 26]. Briefly, a calibration curve was prepared by dilution of a 10% OG stock solution (from 0 to 2% OG). A mixture of 10 µL of each OG concentration, 1 mL of 5% phenol and 2 mL of sulfuric acid was allowed to react for 30 min in a glass vial. Absorbance at 490 nm was measured using a UV-Vis spectrophotometer Beckman Coulter DU-530. Calibration values were compared to those obtained with an AqpZ proteoliposome sample.

2.3. Dynamic light scattering.

Diameter and polydispersion of liposomes were measured by dynamic light scattering (DLS) at 532 nm (Zetasizer ZS, Malvern Panalytical, Worcestershire UK) following established protocols [27].

2.4. Water permeability.

Water permeability was determined following light scattering intensity changes (500 nm) in a SX20 stopped-flow spectrometer (Applied Photophysics, Leatherhead, UK), as described previously [18]. As described above (section 2.1), proteoliposomes were first diluted 10x with PBS, with final tAqpZ of 0.6 µM and OG concentration of 0.03%. This solution was rapidly mixed at 15 °C, unless stated otherwise, with a hyperosmolar PBS solution containing 0.6 M sucrose (total Osm_s 1,021 mmol/kg) to establish a ~0.3 M inwardly directed osmotic gradient. The rate constant, k, was obtained from the average of more than ten individual traces and was fitted with Pro-Data Viewer (Applied Photophysics). Rate constant values were corrected to account for a non-exponential behavior [28] and membrane permeability (P_f) and AqpZ monomer permeability (pf) were calculated as described previously [18, 29].

2.5. Preparation of dye-labeled proteoliposomes.

In labeled samples, AqpZ was chemically labeled with Alexa Fluor™ 555 NHS Ester (Invitrogen™) according to the manufacturer's instructions. Briefly, Alexa Fluor™ 555 (10 mg/mL) was dissolved in dry DMF obtained by $MgSO_4$ filtration. A PD-10 gel filtration column (Bio-Rad, USA) was used to exchange Tris-containing buffer in the AqpZ stock solution (3.2 mg AqpZ) to PBS and 1% OG. The sample was concentrated to 2.6 mg in 150 µL (~15 mg/mL). To the latter, 20 µL of the label in DMF was added slowly and under continuous stirring. This was followed by 2 h incubation with stirring in the dark, at room temperature. The labeled protein was separated from the free dye using a PD-10 gel filtration column (see Supplementary File, Fig. 1). Both species have high absorbance at 555 nm (see fractions 7 and 11 in Supplementary File, Fig. 1A), but only AqpZ has absorbance at 280 nm (fraction 7 in Supplementary File, Fig. 1B). The degree of labeling (DOL) was determined from the absorbances of the protein-dye conjugate, Abs (P*), and the dye, Abs (D), at A_{280} and A_{555}, according to the formula:

$$DOL = \frac{\left(\frac{Abs(P*)_{280} - Abs(D)_{280}}{\varepsilon_{280}}\right)}{\left(\frac{Abs(D)_{555}}{\varepsilon_{555}}\right)} \quad (1)$$

, where ε_{280} and ε_{555} are the extinction coefficients of AqpZ and dye at these wavelengths: 35.1 and 150 $mM^{-1}cm^{-1}$, respectively. DOL of AqpZ was typically 80-90%.

E. coli total lipids were spiked with TopFluor® PC (1-palmitoyl-2-(dipyrromethene boron difluoride) undecanoyl-sn-glycero-3-phosphocholine (Avanti Polar Lipids Inc., Alabama, US) with ε_{500} = 96.9 mM^{-1} cm^{-1}, to reach a non-labeled/labeled lipid molar ratio of 400:1 in chloroform, and the mixture was dried. The labeled AqpZ was added to the dry 'labeled' lipid mixture as described above, to produce labeled AqpZ proteoliposomes (mLPR 400) with an approximate equimolar ratio between labeled lipid and labeled AqpZ monomer. Before collecting UV-Vis spectra to quantify lipid and protein, scattering from liposomes was eliminated by addition of an equal volume of a 6% OG solution. These two dyes were selected initially to perform FRET experiments between lipid (donor) and protein (acceptor). However, these were not successful probably because of the high dilution of the lipid. Absorbance of Alexa Fluor (protein) is not affected by TopFluor (lipid), but the latter partially overlaps with Alexa Fluor (about 26%). To account for this, the absorbance of the lipid dye was corrected (multiplied) by 0.71.

2.6. Hollow fiber and module fabrication. Polyetherimide (PEI, ULTEM™ 1000 resin, Sabic) was used as a hollow fiber substrate fabricated by the conventional dry-jet wet spinning method [30]. The

molecular weight cut-off (MWCO) of the substrate was 300-400 kDa. That is, the membrane rejected 90% of 300-400 kDa particles (Supplementary File, Fig. 2). A molecular weight of 400 kDa corresponds to particles of average diameter ~ 10 nm [31], whereas the proteoliposomes used have an average diameter of 200 nm. N-Methyl-2-pyrrolidone (NMP, >99.5%, Merck Chemicals, Singapore) served as the solvent to dissolve PEI and prepare a dope solution. Five hollow fiber membranes (0.8 mm inner diameter) were sealed in one 0.5-inch diameter Polyvinyl Chloride (PVC) module (L = 30 cm and ø = 0.5 cm).

2.7. Interfacial polymerization.

In a typical module reconstitution experiment (Fig. 1), the stock solution of AqpZ proteoliposomes consisted of 1 mL of 8 mg lipid/mL and 0.65 mg AqpZ/mL, i.e., 400:1 mLPR. First, 1 mL of stock solution was diluted 10x with MPD (m-Phenylenediamine ≧ 99%, Sigma-Aldrich) aqueous solution (1.2 wt % at pH 8) (Fig. 1B). Of these 10 mL, a 1 mL aliquot was taken for further characterization. The remaining 9 mL were used to soak the inner lumen of the fibers in the module for 5 min (Fig. 1C). The solution was flushed out, and typically 90-95% of the volume was recovered. From the flushed volume, a 1 mL aliquot was taken for further characterization. After a rinsing step with cyclohexane (3 min), the inner volume of the fibers was exposed to a 0.15 wt% solution of TMC (trimesoylchloride, >99%, Sigma-Aldrich) in cyclohexane, and left to react for 3 min. The reaction between TMC and MPD at the inner surface of the hollow fibers led to interfacial polymerization (IP). Once fabricated, the modules were soaked in water for at least one day before testing. Samples prepared with inactive mutant AqpZ (R189A) or liposomes with no AqpZ served as negative control. The 1-mL aliquots taken before and after each module-soaking step were kept at 4 °C for further characterization (typically about 4 h after the soaking step).

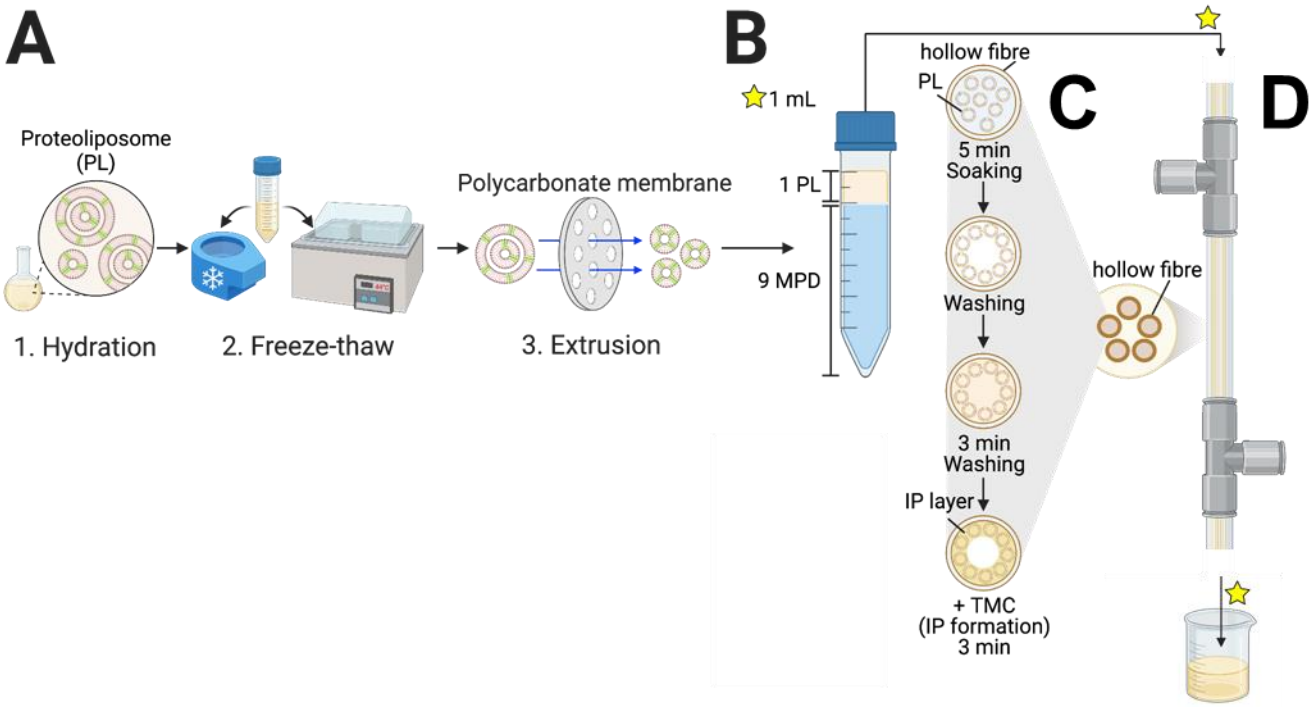

Figure 1. Schematic of AqpZ proteoliposome and module preparation. A) Hydration of dry *E. coli* lipids by addition of AqpZ in OG, to form multilamellar proteoliposomes (1); freeze-thawing (2); manual extrusion to obtain unilamellar proteoliposomes of uniform size (3); B) proteoliposomes diluted 10x in MPD solution; C) soaking of the inner volume of the 5 fibers in the module, followed flushing out, a cyclohexane wash step and addition of TMC to form the IP layer, using the times indicated; D) a 1-mL aliquot was taken before an after soaking the module for further characterization. Graphic created with BioRender.com.

2.8. Retention of lipid and protein inside the modules after IP.

The amount of lipid and protein retained in each module after soaking was estimated from the absorbance at 500 (lipid) and 555 (protein) nm (Beckman-Coulter DU-530 spectrophotometer, 1 cm pathlength) and the measured volumes obtained before and after each module soaking step (Fig. 1), according to the formula:

$$\%\ \text{Recovered} = \frac{ABS_{eluted} \times Vol_{eluted}}{ABS_{initial} \times Vol_{initial}} \qquad (2)$$

2.9. Module evaluation. Sodium chloride (NaCl, Merck Chemicals, Singapore) was used to as the feed solute for RO crossflow testing. All other chemicals or materials were purchased from Sigma-Aldrich (Singapore) unless otherwise stated and used as received. Milli-Q water (Millipore, integrated ultrapure water system) with a resistivity of 18.2 MΩ·cm was used to prepare feed

solutions. Evaluation of membrane separation properties (i.e., the pure water flux and salt rejection) was conducted by low-pressure RO tests using a bench-scale crossflow setup. A high crossflow rate of 0.3 $m \cdot s^{-1}$ was applied to minimize the effect of concentration polarization. The pure water flux test was carried out at 2 bar for at least 1 h until a stable water flux was reached. Salt rejection was measured at 2 bar with a 500 ppm NaCl feed solution using the same cross-flow setup. The water flux, Jv($L \cdot m^2 h^{-1}$), was calculated according to the equation:

$$J_v = \frac{\Delta w}{\Delta t S \rho} \quad (3)$$

Where Δw(kg) is the weight of permeate collected over a certain period of time, Δt is the time interval in hours, S(m^2) is the effective membrane area and ρ($kg \cdot L^{-1}$) is the density of permeate. The salt rejection, R(%), was calculated according to Equation:

$$R = \frac{C_p}{C_f} \times 100\% \quad (4)$$

, where C_f and C_p are the salt concentrations in feed and permeate, respectively.

2.10. Preparation of hollow fiber sections for confocal microscopy. After formation of the IP layer in the hollow fibers, individual hollow fibers were retrieved immediately from the modules and dried for 1 h under vacuum. Sections of these fibers (0.3 cm long) were cut from the beginning (i.e., near the 'input' side), middle and end (near the 'output' side) along the fibers. These fiber fragments were embedded into hot paraffin using metal molds and were attached to a microtome cassette using a Leica EG1150 Embedding Center (Leica Biosystems, Germany) after curing for 1 hour on a cold plate. Thin uniform slices (5 µm thick) of the hollow fibers were obtained using a full-automated rotary microtome RM2265 (Leica Biosystems) and placed onto glass slides for viewing with a confocal microscope. This whole procedure took approximately 6 h after IP formation. Cross-sections of the hollow fibers were viewed with a Zeiss LSM710 confocal microscope equipped with an Airyscan detector using a NeoFluar 10x/0.3 lens. All confocal microscopy experiments were conducted using two lasers, 488 and 561 nm, with emission referred to as "green" (499-548 nm) and "red" (574-627 nm) channels. Alternatively, the hollow fibers were imaged *after* testing the performance of the modules, i.e., three days after formation of the IP layer. In this case, the fibers were first left to dry overnight in the dark before subsequent steps. The cassettes were also stored overnight at -20 °C before obtaining the slices.

2.11 Preparation of bulk interfacial polymer (IP) for confocal microscopy

Equal volumes of 1.2 % m-phenylene diamine (MPD) in water and 0.15 % trimesoyl chloride (TMC) in cyclohexane were mixed together in a small glass container (50 mL). Upon mixing, the polymer formed at the interface of the two solutions. A thick layer of that film was retrieved with two microscope slides. One slide was left to dry on the lab bench, and the other was dried under vacuum. The polymer in the two slides was viewed (i) six hours after drying and (ii) three days after drying.

3. RESULTS

3.1. The proteoliposome sample did not change significantly during preparation. To test if lipid or protein was lost during the preparation of AqpZ proteoliposomes, quantification was performed using the bands in the visible region in labeled proteoliposomes (see section 2.5). Absorbance at 500 or 555 nm did not change significantly, before or after extrusion (Fig. 2, inset). From the absorbances at 500 and 555 nm, the estimated final concentration of labeled lipid and AqpZ were indeed equimolar as expected (17.3 ± 2.1 µM and 17.4 ± 2 µM, although lower than the expected nominal value of 24 µM. Thus, both lipid and AqpZ concentrations were smaller than expected, even before extrusion, but the extrusion steps did not result in losses of either fraction. We note that the 280 nm band amplitude was about five times larger than expected (equivalent to 122 µM AqpZ, instead of the expected 25 µM). This is caused by a contribution of *E. coli* lipids in the UV around 270 nm, possibly because of the presence of ubiquinone or polyunsaturated lipids. We found that this contribution differed from batch to batch of commercial *E. coli* lipid (not shown). In any case, the absorbance at 280 nm did not change significantly in the labeled samples or in the unlabeled (not shown) ones.

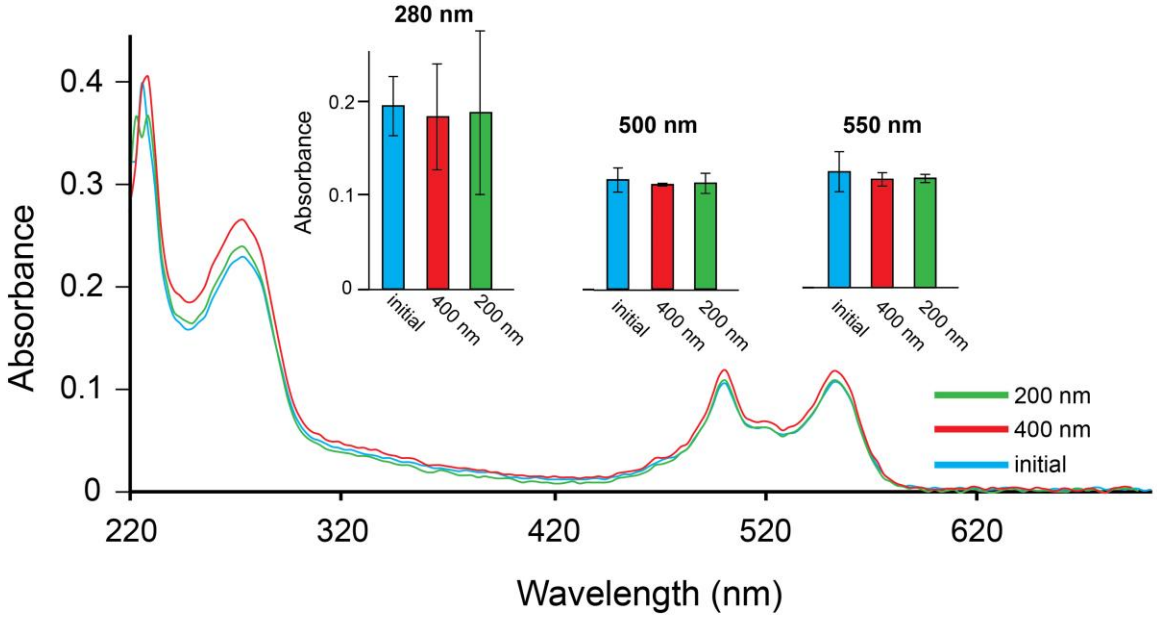

Figure 2. Sample quantification during labeled proteoliposome preparation. (A) UV-Visible spectra of proteoliposomes before (initial), after extrusion through 400 nm pores (400 nm)

and after extrusion through 200 nm pores (200 nm). The inset shows the variation of the absorbance in these three samples at 280, 500 and 550 nm for three independent measurements. The band at 280 nm could not be used to measure AqpZ concentration because *E. coli* lipids showed strong absorption in that region (not shown).

3.2. Visualization of AqpZ and lipid at the inner surface of the hollow fibers after IP formation. After soaking and IP layer formation, the presence and localization of AqpZ and lipid within the hollow fibers was determined using confocal microscopy. This was performed in a half-inch module containing five hollow fibers (Fig. 3A-B). Each one of the fibers (Fig. 3C) was embedded in resin (Fig. 3D, and see Materials and Methods section 2.10) and imaged. Although slices were obtained for each fiber in several modules at the three regions shown in Fig. 3E, for simplicity only representative slices corresponding to the middle of one module are shown. Red (protein) and green (lipid) emission was clearly localized at the inner surface of the fibers (Fig. 3F-H, white arrows). In contrast, hollow fibers reconstituted with unlabeled AqpZ proteoliposomes did not produce any emission in the red channel (Fig. 3I) and only a faint emission in the green channel (Fig. 3J). Overlap of the two channels is shown in panels H and K. Other slices captured at these and other positions in other fibers and other modules were similar and are not shown. Thus, these results demonstrate that both AqpZ and lipid are localized at the inner surface of the hollow fibers and suggest their capture or encasing by the IP formation. Regarding the residual fluorescence observed in panel J, we later found (see below) that it was not caused by the hollow fiber material or by proteoliposomes, but by one or more chemicals present after IP formation.

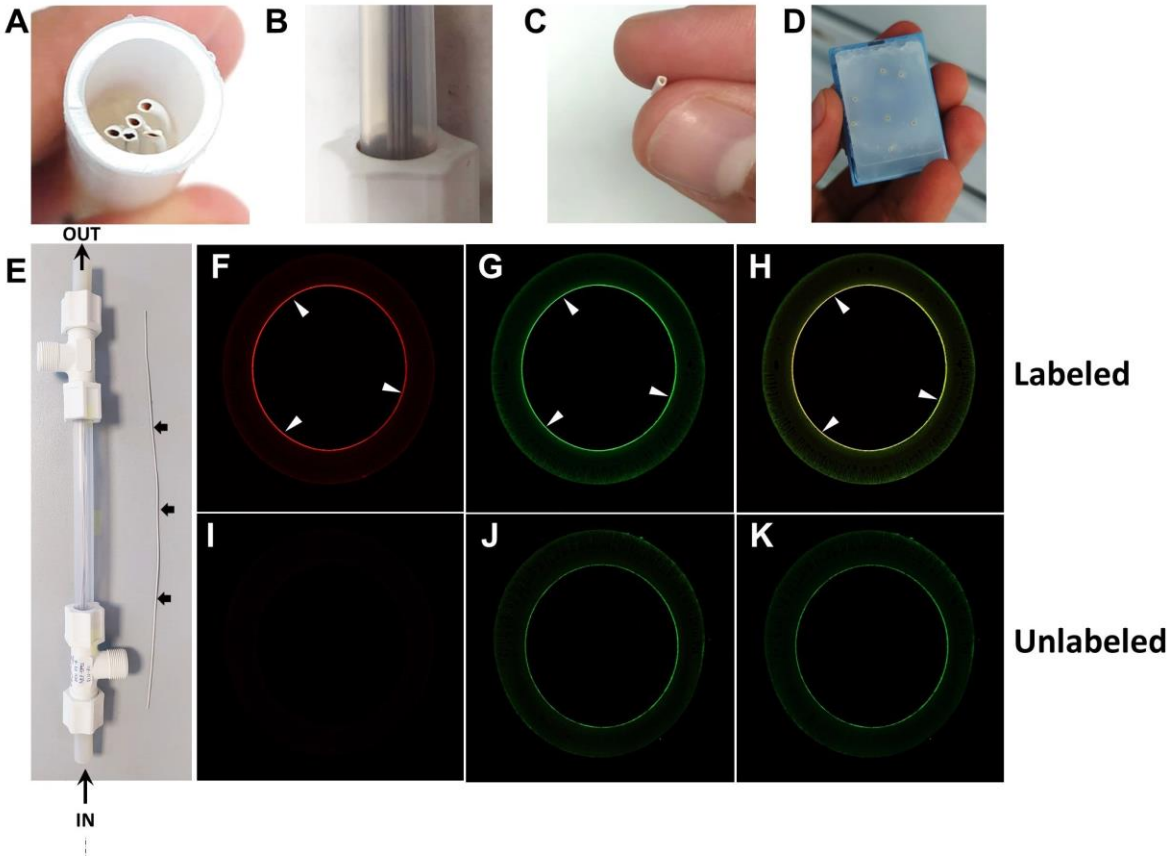

Figure 3. Visualization of labeled AqpZ and lipid in hollow fibers approximately six hours after IP formation. (A-B) Half-inch module containing five identical hollow fibers; (C-D) one of these fibers before and after embedding in the resin (D); (E) half-inch module, where 'in' and 'out' represent the direction of water flow and arrows show cutting points; (F-H) fluorescence from a section of a hollow fiber reconstituted with labeled proteoliposomes; (I-K) same for a section of a hollow fiber where unlabeled AqpZ proteoliposomes were used.

3.3. Fluorescence from hollow fibers treated with unlabeled proteoliposomes. We investigated the fact that even hollow fibers treated with unlabeled proteoliposomes produced a faint fluorescence in the green channel 6 h after IP (Fig. 3J). Untreated hollow fibers produced no fluorescence (Supplementary File, Fig. 3A-C). However, when hollow fibers were imaged after testing module performance (water permeability and salt rejection), which typically required a total of three days until the sample was ready for the microscope, both red and green fluorescence could be clearly observed even when unlabeled proteoliposomes were used (Supplementary File, Fig. 3D-F). However, this unwanted fluorescence was not limited to the inner surface, but was also found inside the walls and at the outer edge of the

hollow fibers. When fibers reconstituted with labeled proteoliposomes were imaged in the same conditions (three days after IP formation) a similar result was obtained, although with a more intense fluorescence at the inner surface of the fiber, consistent with the presence of labeled lipid and protein in that sample (Supplementary File, Fig. 3G-I).

To discount the possibility that proteoliposomes partially leaked through the hollow fiber walls, we produced hollow fibers with half the pore diameter (around 200 kDa cut-off), as small as technically possible using this technology. However, results using these narrower-pore hollow fibers also showed fluorescence at the outer edge of the fibers after three days (not shown). To test if this fluorescence was caused by leftover MPD in the hollow fiber after IP formation, we solubilized MPD in water (2.5% MPD). The solution was initially colorless but acquired a yellowish color after three days, possibly because of oxidation. Howewer, although it produced a broad spectrum in the visible region (see Supplementary File, Fig. 4), no fluorescence was observed when excited at any of the wavelengths used in the confocal microscopy experiment (not shown). Similarly, a TMC solution in cyclohexane was colorless for up to three days, and did not produce any fluorescence (not shown). Although investigation of the origin of this fluorescence is out of the scope of the present manuscript, IP polymer formed in a small container (see section 2.11) was imaged in the confocal microscope 6 h after its formation. Consistent with our previous observations when we imaged modules reconstituted with unlabeled liposomes 6 h after IP formation (Fig. 3J), no fluorescence was observed in the red channel, but some could be detected in the green channel (Supplementary File, Fig. 5A-B). Fluorescence was undetectable if the sample was left to dry under vacuum (Supplementary File, Fig. 5C-D), suggesting that it derives from an oxidation product. Interestingly, fluorescence was much more intense after three days (Supplementary File, Fig. 5E-F) and was also detectable in the red channel, again consistent with our observations in module sections. As in the ‘6h sample’, the intensity of emission was clearly reduced when the sample was not exposed to oxygen (Supplementary File, Fig. 5G-H). Therefore this demonstrates that this evolving fluorescence derives from the IP reaction products and not from the lipid or AqpZ.

3.4. Quantification of lipid and protein retained in hollow fibers after module soaking. UV-Vis spectra of samples collected before (input, I) and after soaking the modules (output, O) (Fig. 4A) show the presence of both lipid and protein (bands at 500 and 555 nm, respectively) and a very high absorption below 350 nm, due to MPD. A sample corresponding to the

cyclohexane wash (Fig. 1) only showed a band at 290 nm, attributed to MPD. This indicates that both fluorescent dyes (in lipid and protein) survived the exposure to MPD because we could monitor their presence even hours after module reconstitution. . We note that the MPD solution slowly evolved a colored compound over time, over several hours. However, after 4 h it only amounted to approximately 0.007 absorbance units at 550 nm (Supplementary File, Fig. S4), whereas our visible measurements were in the range 0.1-0.2. On average, absorbance values at 500 and 555 nm after soaking were lower than before soaking (Fig. 4A). From absorbance and volume values, and after a correction for the partial overlap of the two fluorophores (a 17/24 = 0.71 factor, see section 2.5), the average moles of lipid and protein retained in the modules was estimated to be 1.5 ± 1.6 nmoles (~17%) and 1.4 ± 1.1 (~19%), respectively (Fig. 4B). This loss is consistent with the 0.5-1 mL solution lost in each module after the soaking step and with the total inner volume of the five hollow fibers combined (~0.75 mL). This volume is likely then flushed out with the cyclohexane washing step and quantification of the actual protein and lipid available during IP formation could not be estimated.

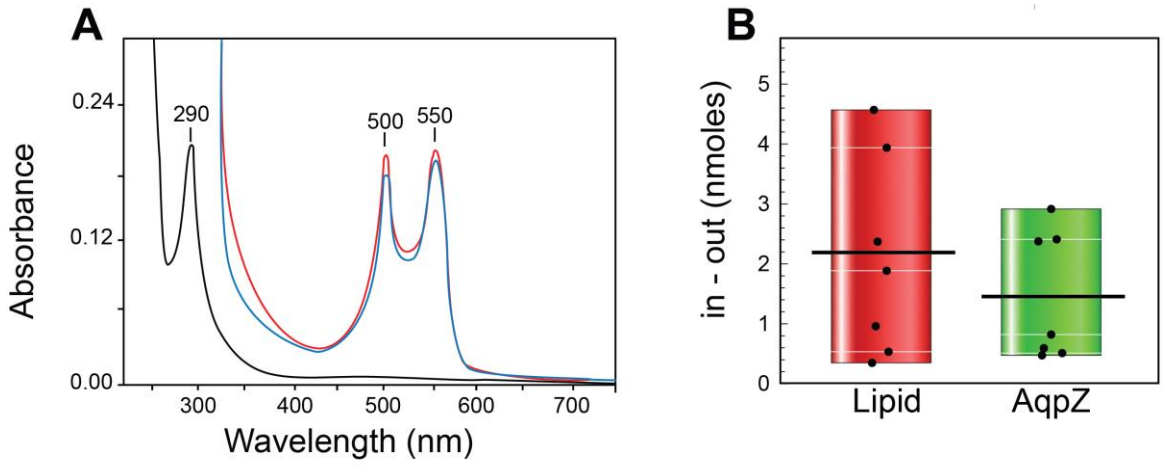

Figure 4. Lipid and protein retained in the modules. (A) Representative spectra corresponding to AqpZ proteoliposomes mixed with MPD before soaking (input, blue) and after soaking (output, red), and a sample obtained after cyclohexane wash containing MPD alone (black); (B) difference between the nanomoles of lipid and protein, before and after soaking, based on the absorbances of the solutions at 500 nm and 555 nm, respectively. Values for individual modules (five fibers each) are shown as black dots. GlassQuantile plots were obtained with Mathematica v. 12.3.1 (Wolfram Research, Inc., Champaign, IL), where short white

horizontal lines represent 25, 50 and 75% quantiles of the data and long lines represent the averages.

3.5. Effect of labeling in stopped-flow experiments. Next, we tested the performance of these modules. However, we noticed that in stopped flow experiments, labeled proteoliposomes showed lower permeability than expected (see below). To test if this lower permeability was caused by AqpZ or lipid labeling, we compared proteoliposomes reconstituted with either labeled AqpZ or labeled lipid at different LPRs (Fig. 5). As expected, in unlabeled samples (first and fourth bar), LPR 400 proteoliposomes were about twice as permeable as LPR 800 proteoliposomes, on account of their higher AqpZ density. Similar results were obtained when only the protein was labeled (second and fifth bar), with P_f values similar to those obtained for unlabeled samples. Also, the P_f of LPR 400 samples with equal contribution of labeled and unlabeled AqpZ (third bar) was similar to that of LPR 400 liposomes made entirely with unlabeled AqpZ. Overall, this indicates that labeling of AqpZ does not have an effect on the shrinking rate of liposomes observed in stopped-flow experiments.

However, when lipid was labeled (sixth and seventh bars), LPR 400 liposomes showed even lower permeability than LPR 800 samples where only AqpZ was labeled (fifth bar). These results suggest that it is the labeled lipid that affects liposome shrinking in the stopped-flow experiment. This is surprising since the ratio of labeled to unlabeled lipid is 1:400, but we hypothesize that labeling may affect the bulk lipid matrix rigidity. However, since the later probably plays no major role in module performance, we expected normal module performance when using labeled proteoliposomes (see below).

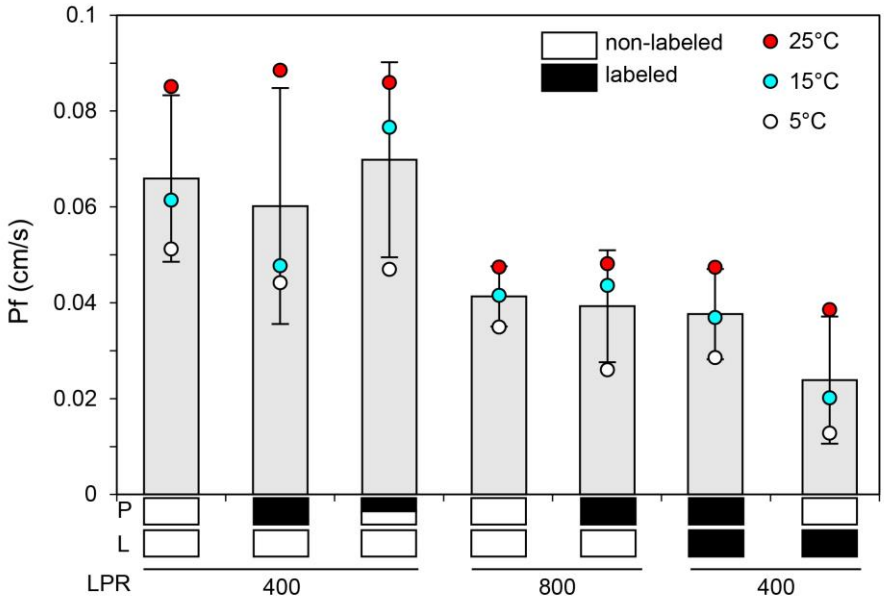

Figure 5. Effect of labeling on the permeability of AqpZ proteoliposomes in stopped flow measurements. For each condition, experiments were performed at the three temperatures indicated (top right) and the bars are the averages of these three values. The LPR in indicated at the bottom, and whether protein (P) or lipid (L) was labeled is indicated by white (non-labeled) and black (labeled) rectangles. A mixed white/black rectangle indicates a 50/50 mixture of labeled and unlabeled AqpZ.

3.6. Module performance. The performance of the modules using labeled proteoliposomes (WT-L) was compared to those that used unlabeled samples of WT AqpZ (WT-UL), R189A mutant (R189A) or just *E. coli* lipid (Lipid). These results are summarized in Table 1 and Fig. 6. Despite the labeling, modules reconstituted using labeled AqpZ proteoliposomes showed good water permeability (~ 8.1 LMH/bar), comparable to those reconstituted with unlabeled AqpZ (WT-UL) proteoliposomes (~ 8.9 LMH/bar). The difference was not significant at $p = 0.05$ (Fig. 6A). To test the dependence of module performance on AqpZ water channel activity, six modules were tested with proteoliposomes containing R189A AqpZ mutant [29]. This mutant has a permeability about six times lower than wild type AqpZ (Supplementary File, Fig. 6). Modules reconstituted with R189A showed significantly lower permeability than those reconstituted with WT AqpZ, but higher than those where only lipid was used (5.6 versus 3.7 LMH/bar, respectively) (Fig. 6A). Neverthless, this small difference is surprising since the permeability of lipid-only liposomes is about 5-10x lower than that of R189A liposomes (Supplementary File, Fig. 7).

In terms of salt rejection (Fig. 6B), modules reconstituted with unlabeled AqpZ (WT-UL) performed better than those that used labeled AqpZ (WT-L). When compared with labeled or unlabeled WT AqpZ, salt rejection was not worse when using the R189A mutant. However, absence of protein (sample 'Lipid') reduced salt rejection, compared to WT-L, WT-UL or R189A modules. These results indicate that module water permeability is arranged in the order WT-UL > WT-L > R189A > Lipid. At first glance, this suggests that module permeability properties are linked to the permeability of membranes used. In terms of salt rejection, use of unlabeled AqpZ has a slight advantage over labeled AqpZ, but it is not affected by the use of the R189A mutant. However, modules reconstituted with only lipid are clearly worse than those that used AqpZ (WT-L, WT-UL or R189A).

Sample	n	Permeability (LMH/bar)	Salt Rejection (%)
WT-L	7	**8.1 ± 0.8**	**94.0 ± 0.8**
WT-UL	6	**8.9 ± 0.8**	**95.5 ± 1.2**
L + UL	13	**8.5 ± 0.9**	**94.7 ± 1.2**
R189A	6	**5.6 ± 1.7**	**94.5 ± 1.8**
Lipid	7	**3.7 ± 1.1**	**91.3 ± 2.2**

Table 1. Permeability and salt rejection of the modules. Legends indicate modules incorporating labeled (WT-L) AqpZ, unlabeled (WT-UL) AqpZ, average of all modules with labeled and unlabeled AqpZ (L+UL, AqpZ R189A mutant or liposomes with only lipid (Lipid). The number of modules (n) tested in each case is indicated.

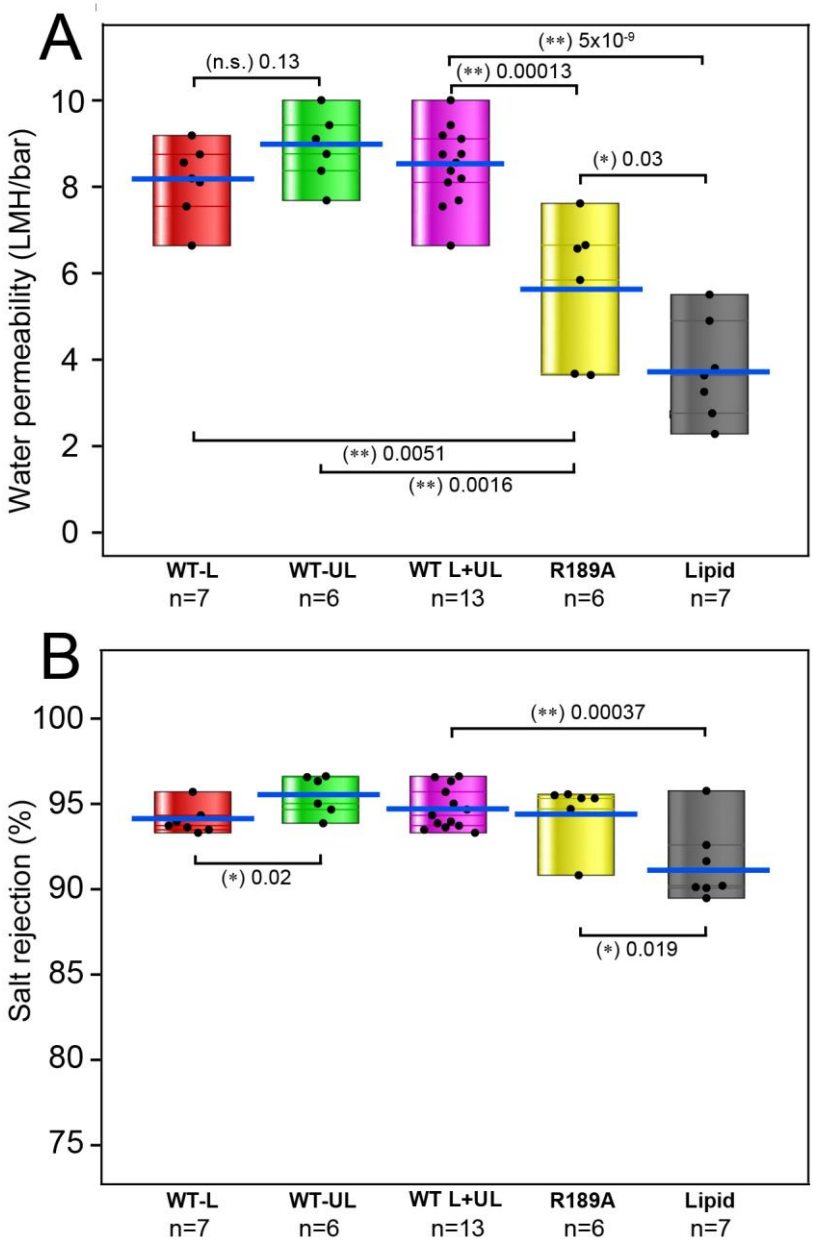

Figure 6. Performance of reconstituted modules. Labels have same meaning as in Table 1. Values for individual modules (five fibers each) are shown as black dots. GlassQuantile plots were obtained with Mathematica v. 12.3.1 (Wolfram Research, Inc., Champaign, IL), short and long horizontal lines have the same meaning as in Fig. 4. The numbers represent p values in more stringent two-tailed test pairwise comparisons, where $p < 0.05$ is considered statistically significant. The symbols *, **, and n.s. represent $p<0.05$, $p<0.01$ and 'not significant', respectively. The number of modules used for each sample type is shown at the bottom. When no comparison is shown, results were not significantly different at $p = 0.05$.

3.7. Long term module performance. We have shown that AqpZ and lipid are co-localized with the IP layer (Fig. 3) and that module permeability seems somewhat correlated with membrane permeability (Fig. 6). However, both lipid and AqpZ are expected to be degraded with time, therefore if module performance requires a functioning AqpZ in a proper lipid environment, this seems to be in conflict with reports where, using this same procedure, modules can perform unaffected for several months [18, 23]. To test this, we incubated a solution of AqpZ proteoliposomes at room temperature and we monitored the kinetics of degradation using FTIR spectroscopy over more than five months (Fig. 7). These spectra show a reduction in the intensity corresponding to lipid ester C=O bond at 1740 cm^{-1} and a gradual increase in β-structure at 1635 cm^{-1}.

From these spectra, three features were quantified: α-helix percentage, lipid ester bond and α-helix/β-structure ratio (Fig. 8A). The band corresponding to lipid ester C=O bond (1741 cm^{-1}) decayed with a half-life of about one month (34 days), consistent with ester bond hydrolysis. At about five months, this band had disappeared almost completely. Features related to AqpZ integrity changed even faster; the α-helical structure content and the α/β ratio ended in a plateau in about 1-2 months.

Since the reconstituted modules are kept at room temperature, it is reasonable to assume that if these same processes take place inside the IP layer, and performance critically depends on AqpZ water channel activity, initial permeability and salt rejection would not be maintained for more than 2-3 weeks.

To test this, in parallel with the above experiment, we tested two half-inch modules reconstituted independently with unlabeled AqpZ proteoliposomes, and performance was evaluated over 5 months at the times indicated by the dotted lines in Fig. 8A and dots in Fig. 8B-C. The initial performance of the two modules was higher than 8 LMH/bar, whereas salt rejection was around 95%. Over five months, the modules were tested periodically, only at the times indicated, for one day, and no chemical cleaning was done. Water permeability was somewhat lower, but still above 8 MHL/bar after five months, whereas salt rejection was reduced to around 92-93%.

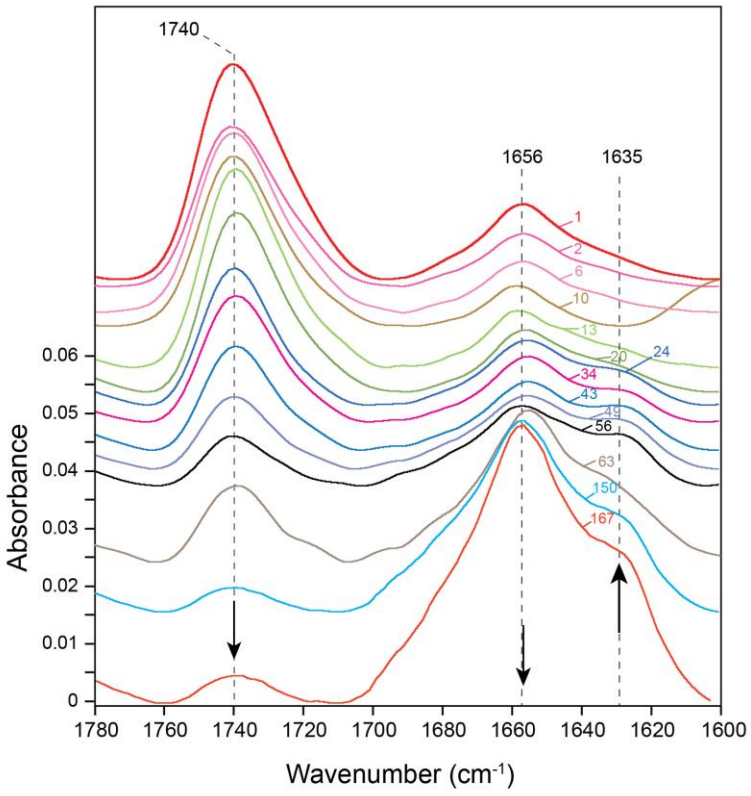

Figure 7. Ageing of AqpZ proteoliposomes at room temperature. (A) IR spectra of AqpZ proteoliposomes stored at room temperature, where each spectrum is labeled with the number of days since incubation started. Arrows indicate direction of change.

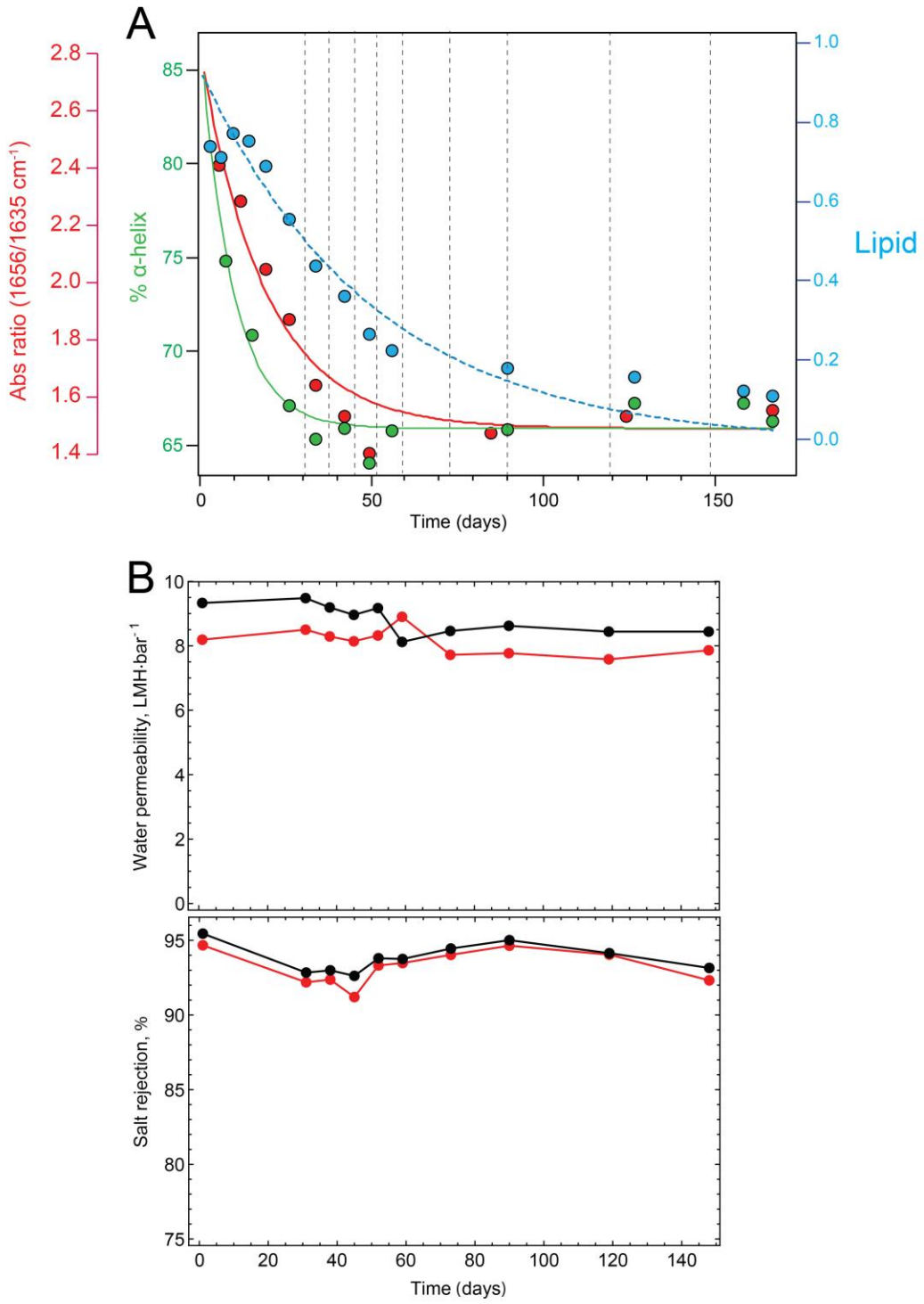

Figure 8. Kinetics of degradation and module performance over several months. (A) Evolution of lipid band area, % of α-helix structure and ratio α-helix/β-structure taken as the ratio of intensities at 1655 and 1635 cm^{-1}, respectively, based on the data in Fig. 7. Dots represent individual measurements whereas lines represent fitted mono-exponential decay curves. Vertical dotted lines represent the times at which the performance of the modules were tested (see panels B and C); (B-C) permeability (B) and salt rejection (C) in

the two modules immediately after IP formation (day 0) and after a number of days indicated (dots). Lines are only shown to guide the eye.

4. Discussion.

4.1. Module permeability is not consistent with major AqpZ water channel contribution. The confocal microscopy results clearly show that both lipid and AqpZ are retained in the inner surface of the hollow fiber, likely co-localized with the IP layer. The fluorescence observed, measured a few hours after IP formation, did not spread to other parts of the hollow fiber. This is consistent with the MWCO of the substrate, 300-400 kDa, equivalent to a particle size of about 10-11 nm in diameter. For example, the effective hydrodynamic diameter of HIV Env protein (500 kDa, PDB: 4NCO) is 11.5 nm, according to the HydroPro algorithm [32]. This size is more than one order of magnitude smaller than the liposomes used (150-200 nm). While both components are present, the actual amount of lipid and protein retained at the inner surface of the hollow fibers before IP is difficult to quantify. Ideally, one should achieve a complete coverage of a surface with liposomes to maximize permeability, referred to a '1x coverage'. Based on liposome size and either cross-sectional area of lipids, e.g., 50-65 $Å^2$ [33, 34] or bilayer thickness [22, 35], ~ 2 µg lipid/cm^2 is required for this. If one considers a model where the available surface for water flux is a series of side-to-side non-overlapping half-spheres covering the entire surface [36], for 150 nm liposomes this would require ~44 liposomes/ $µm^2$ (Equation 1 in Supplementary File) which, independent from vesicle radius, would represent an available surface of 1.57 $µm^2$ for each 1 $µm^2$.

From the membrane permeability value (P_f) obtained in the stopped-flow (~440 µm/s), one can derive the permeability (A) [36] of the membranes (see Equation 2 in Supplementary File) as 0.32 µm s^{-1} bar^{-1}. Since in that model water would have to cross the liposome twice (two half spheres), the membrane permeability is halved, i.e., 0.16 µm s^{-1} bar^{-1}. Corrected by the surface factor, 1.57, this is equivalent to 0.25 µm s^{-1} bar^{-1}, or 0.9 LMH bar^{-1}. Therefore, even with 1x coverage, the contribution of the water channel activity of AqpZ at this LPR 400 ratio is expected to be roughly < 10% of the one observed for modules reconstituted with WT AqpZ (8-9 LMH bar^{-1}). The low density of protein is clearly a limitation [17]. From the area of each AqpZ tetramer (36 nm^2, PDB 1RC2) and a 65 $Å^2$ estimate for lipid area, the AqpZ density is only 1,800 AqpZ tetramers/$µm^2$ (2,800 after 1.57x correction), whereas ~

40,000 tetramers could be fitted if they were maximally arranged side-to-side, in a 2D-crystallization fashion. In the latter case, permeability due to AqpZ could increase more than one order of magnitude, to higher than 10 LMH/bar.

In a recent report, polymer surfaces were exposed to liposome solutions containing 50 or 250 times excess lipid than the 2 μg lipid/cm^2 required for 1x coverage, and phosphorous deposited on the surface was quantified by ICP-MS [22]. The analyzed membranes contained 1.35% and 1.06 % of total phosphorous, respectively, equivalent to a coverage of approximately 65% (50 x 0.0135) and 250% (250 x 0.01). In our conditions, we exposed the surface of the hollow fiber to a '100x' excess solution, expected from [22] to produce a 100 % coverage. In any case, we show that even in the most favorable case of 1x coverage, the AqpZ water channel contribution would be <10% of the one observed in the modules tested.

4.2. Comparison of modules made with WT, R189A and lipid-only proteoliposomes. From our stopped-flow results, the membrane permeability (P_f) for wild type AqpZ, R189A mutant and just-lipid proteoliposomes was ~440 μm/s, ~88 μ/s and ~15 μm/s, respectively, i.e., WT AqpZ membranes are ~25x more permeable than lipid-only membranes (Supplementary Fig. 7). However, the presence of WT AqpZ only increased module permeability by a factor of 2.3 from 3.7 ± 1.1 LMH/bar to ~8.5 ± 0.9 LMH/bar. Equally, the permeability of modules reconstituted with AqpZ mutant (R189A) (5.6 ± 1.7 LMH/bar) was only ~1.5 lower than those that used WT AqpZ. These data, combined with the fact that complete coverage in these conditions would only account for ~ 1 LMH/bar for WT AqpZ, indicates that AqpZ water channel activity in this system does not have a major role in module performance.

4.3. Long term module performance is inconsistent with fast proteoliposome degradation at room temperature. The conclusion above is supported by our long-term performance experiment. Indeed, while module performance only changed slighty over the course of five months, a proteoliposome solution showed degradation with a half-life of 1-2 weeks at room temperature. Even in the most optimal case of 1x coverage, one would expect to see a small reduction in water permeability over time of ~ 1 LMH/bar. It could be hypothesized that AqpZ and lipids are somehow stabilized after entrapment in the IP layer and do not suffer the same degradation observed in solution, or that AqpZ is still able to function even when most

bulk lipids are degraded, with key lipids, i.e., cardiolipin, still tightly bound to the protein [14, 37]. However, we think more likely that the coverage is lower than 100%.

Regardless of the hypothesis, it is clear that most of the module performance is driven by the IP layer, which is far more stable than either lipid or protein components. Another question then is the origin of the differences observed in the performance of modules reconstituted with labeled or unlabeled WT AqpZ, R189A mutant and lipids. As discussed above, even considering a 1x coverage, these differences cannot be justified considering relative membrane permeabilities. We hypothesize that these differences are due to morphological changes in the polyamide layer caused by the presence of lipid and protein components. In addition, although three of these samples contain the same protein, uniform labeling of AqpZ likely changes its stability relative to the unlabeled species. Similarly, WT AqpZ forms tetramers in SDS at room temperature, whereas the R189A mutant forms monomers in the same conditions (see gel in Supplementary File S8). Thus, module performance changes may depend on the physico-chemical characteristics of these additives. Overall, it is expected that increasing AqpZ density should improve performance, but this is difficult to achieve using proteoliposomes.

Credit author statement:

Loveena Sharma: investigation, formal analysis; Li Ye: investigation, resources; Clare Yong: investigation; Ramya Seetharaman: resources; Kai Ling: resources; Wahyu Surya: investigation; Wang Rong: funding acquisition, resources; Jaume Torres: conceptualization, supervision, formal analysis, visualization, writing, funding acquisition.

ACKNOWLEDGEMENTS

Funding: This research was funded by grants awarded to J.T. by the Singapore Ministry of Education (MOE) Tier 1 grant RT13/19 and National Research Foundation (NRF) Industry Alignment Fund- Pre-positioning (IAF-PP) awarded to W.R.

REFERENCES

[1] M. Elimelech, W.A. Phillip. The future of seawater desalination: Energy, technology, and the environment, Science, 333 (2011) 712-717.

[2] L. Cao, X. He, Z. Jiang, X. Li, Y. Li, Y. Ren, L. Yang, H. Wu. Channel-facilitated molecule and ion transport across polymer composite membranes, Chem Soc Rev, 46 (2017) 6725-6745.

[3] G. Benga, O. Popescu, V. Borza, V.I. Pop, A. Muresan, I. Mocsy, A. Brain, J.M. Wrigglesworth. Water permeability in human erythrocytes: identification of membrane proteins involved in water transport, European Journal of Cell Biology, 41 (1986) 252-262.

[4] B.M. Denker, B.L. Smith, F.P. Kuhajda, P. Agre. Identification, purification, and partial characterization of a novel M(r) 28,000 integral membrane protein from erythrocytes and renal tubules, J Biol Chem, 263 (1988) 15634-15642.

[5] G.M. Preston, T.P. Carroll, W.B. Guggino, P. Agre. Appearance of water channels in Xenopus oocytes expressing red cell CHIP28 protein, Science, 256 (1992) 385-387.

[6] T. Gonen, P. Sliz, J. Kistler, Y. Cheng, T. Walz. Aquaporin-0 membrane junctions reveal the structure of a closed water pore, Nature, 429 (2004) 193-197.

[7] H. Sui, B.-G. Han, J.K. Lee, P. Walian, B.K. Jap. Structural basis of water-specific transport through the AQP1 water channel, Nature, 414 (2001) 872-878.

[8] Y. Hiroaki, K. Tani, A. Kamegawa, N. Gyobu, K. Nishikawa, H. Suzuki, T. Walz, S. Sasaki, K. Mitsuoka, K. Kimura, A. Mizoguchi, Y. Fujiyoshi. Implications of the aquaporin-4 structure on array formation and cell adhesion, J Mol Biol, 355 (2006) 628-639.

[9] R. Horsefield, K. Norden, M. Fellert, A. Backmark, S. Tornroth-Horsefield, A.C. Terwisscha Van Scheltinga, J. Kvassman, P. Kjellbom, U. Johanson, R. Neutze. High-resolution x-ray structure of human aquaporin 5, Proc Natl Acad Sci USA, 105 (2008) 13327-13332.

[10] E. Tajkhorshid, P. Nollert, M.Ã. Jensen, L.J.W. Miercke, J. O'Connell, R.M. Stroud, K. Schulten. Control of the selectivity of the aquaporin water channel family by global orientational tuning, Science, 296 (2002) 525-530.

[11] J.K. Lee, D. Kozono, J. Remis, Y. Kitagawa, P. Agre, R.M. Stroud. Structural basis for conductance by the archaeal aquaporin AqpM at 1.68 Ã…, Proc Natl Acad Sci USA, 102 (2005) 18932-18937.

[12] D.F. Savage, R.M. Stroud. Structural Basis of Aquaporin Inhibition by Mercury, J Mol Biol, 368 (2007) 607-617.

[13] L.B. Shi, W.R. Skach, A.S. Verkman. Functional independence of monomeric CHIP28 water channels revealed by expression of wild-type mutant heterodimers, J Biol Chem, 269 (1994) 10417-10422.

[14] C.L. Tan, J. Torres. Positive cooperativity in the activation of E. coli aquaporin Z by cardiolipin: Potential for lipid-based aquaporin modulators, Biochimica et biophysica acta. Molecular and cell biology of lipids, 1866 (2021) 158899.

[15] P. Agre. The aquaporin water channels, Proc Am Thorac Soc, 3 (2006) 5-13.

[16] U.K. Eriksson, G. Fischer, R. Friemann, G. Enkavi, E. Tajkhorshid, R. Neutze. Subangstrom Resolution X-Ray Structure Details Aquaporin-Water Interactions, Science, 340 (2013) 1346-1349.

[17] C.J. Porter, J.R. Werber, M. Zhong, C.J. Wilson, M. Elimelech. Pathways and Challenges for Biomimetic Desalination Membranes with Sub-Nanometer Channels, ACS nano, 14 (2020) 10894-10916.

[18] X. Li, S. Chou, R. Wang, L. Shi, W. Fang, G. Chaitra, C.Y. Tang, J. Torres, X. Hu, A.G. Fane. Nature gives the best solution for desalination: Aquaporin-based hollow fiber composite membrane with superior performance, J Memb Sci, 494 (2015) 68-77.
[19] Y. Zhao, C. Qiu, X. Li, A. Vararattanavech, W. Shen, J. Torres, C. Hélix-Nielsen, R. Wang, X. Hu, A.G. Fane, C.Y. Tang. Synthesis of robust and high-performance aquaporin-based biomimetic membranes by interfacial polymerization-membrane preparation and RO performance characterization, J Memb Sci, 423-424 (2012) 422-428.
[20] X. Li, R. Wang, F. Wicaksana, C. Tang, J. Torres, A.G. Fane. Preparation of high performance nanofiltration (NF) membranes incorporated with aquaporin Z, J Memb Sci, 450 (2014) 181-188.
[21] W. Xie, F. He, B. Wang, T.S. Chung, K. Jeyaseelan, A. Armugam, Y.W. Tong. An aquaporin-based vesicle-embedded polymeric membrane for low energy water filtration, Journal of Materials Chemistry A, 1 (2013) 7592-7600.
[22] H.X. Gan, H. Zhou, H.J. Lee, Q. Lin, Y.W. Tong. Toward a Better Understanding of the Nature-Inspired Aquaporin Biomimetic Membrane, Langmuir, 35 (2019) 7285-7293.
[23] S. Qi, R. Wang, G.K.M. Chaitra, J. Torres, X. Hu, A.G. Fane. Aquaporin-based biomimetic reverse osmosis membranes: Stability and long term performance, J Memb Sci, 508 (2016) 94-103.
[24] F. Olson, C.A. Hunt, F.C. Szoka, W.J. Vail, D. Papahadjopoulos. Preparation of liposomes of defined size distribution by extrusion through polycarbonate membranes, BBA - Biomembranes, 557 (1979) 9-23.
[25] B. Lorber, J.B. Bishop, L.J. DeLucas. Purification of octyl beta-D-glucopyranoside and re-estimation of its micellar size, Biochimica et biophysica acta, 1023 (1990) 254-265.
[26] M. Dubois, K. Gilles, J.K. Hamilton, P.A. Rebers, F. Smith. A colorimetric method for the determination of sugars, Nature, 168 (1951) 167.
[27] W. Surya, S. Chooduang, Y.K. Choong, J. Torres, P. Boonserm. Binary toxin subunits of lysinibacillus sphaericus are monomeric and form heterodimers after in vitro activation, PLoS ONE, 11 (2016).
[28] C. Hannesschlager, T. Barta, C. Siligan, A. Horner. Quantification of Water Flux in Vesicular Systems, Sci Rep, 8 (2018) 8516.
[29] M.J. Borgnia, D. Kozono, G. Calamita, P.C. Maloney, P. Agre. Functional reconstitution and characterization of AqpZ, the E. coli water channel protein, J Mol Biol, 291 (1999) 1169-1179.
[30] R. Wang, L. Shi, C.Y. Tang, S. Chou, C. Qiu, A.G. Fane. Characterization of novel forward osmosis hollow fiber membranes, J Memb Sci, 355 (2010) 158-167.
[31] H.P. Erickson. Size and shape of protein molecules at the nanometer level determined by sedimentation, gel filtration, and electron microscopy, Biol Proced Online, 11 (2009) 32-51.
[32] J. Garcia De La Torre, M.L. Huertas, B. Carrasco. Calculation of hydrodynamic properties of globular proteins from their atomic-level structure, Biophys J, 78 (2000) 719-730.
[33] W. Ding, M. Palaiokostas, W. Wang, M. Orsi. Effects of Lipid Composition on Bilayer Membranes Quantified by All-Atom Molecular Dynamics, J Phys Chem B, 119 (2015) 15263-15274.
[34] S. Tristram-Nagle, Y. Liu, J. Legleiter, J.F. Nagle. Structure of gel phase DMPC determined by X-ray diffraction, Biophys J, 83 (2002) 3324-3335.
[35] J.H. van Zanten. Unilamellar Vesicle Diameter and Wall Thickness Determined by Zimm's Light Scattering Technique, Langmuir, 10 (1994) 4391-4393.
[36] M. Grzelakowski, M.F. Cherenet, Y.X. Shen, M. Kumar. A framework for accurate evaluation of the promise of aquaporin based biomimetic membranes, J Memb Sci, 479 (2015) 223-231.

[37] A. Laganowsky, E. Reading, T.M. Allison, M.B. Ulmschneider, M.T. Degiacomi, A.J. Baldwin, C.V. Robinson. Membrane proteins bind lipids selectively to modulate their structure and function, Nature, 510 (2014) 172-175.

Supplementary File.

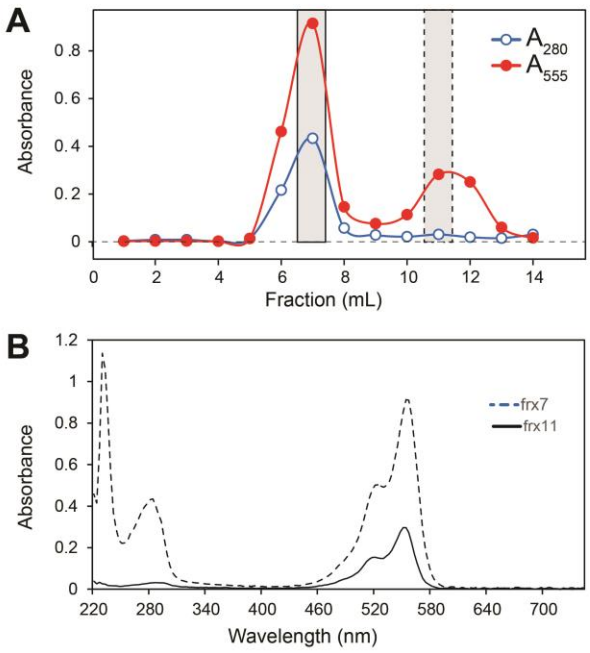

Supplementary Figure 1. Labeling of AqpZ. (A) Size exclusion chromatography of AqpZ after incubation with Alexa-555 dye, monitored at 280 and 555 nm; (B) UV-Vis spectra of fractions 7 (labeled AqpZ) and 11 (free dye) corresponding to the two peaks in (A). Both labeled AqpZ and free dye absorb at 555 nm (fractions 7 and 11), but only AqpZ absorbs strongly at 280 nm (fraction 7).

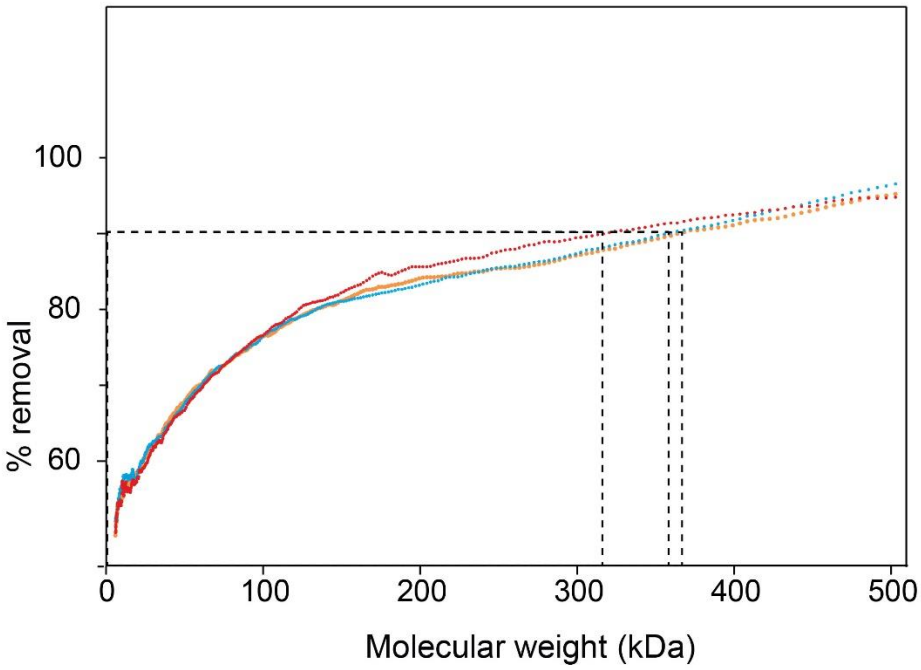

Supplementary Figure 2. Molecular weight cut-off (MWCO) of hollow fiber support. Dextran solutions with molecular weights ranging from 6-500 k were evaluated after examining composition of feed and draw. The MWCO was taken as the molecular weight of dextran rejected >90% (see dotted line).

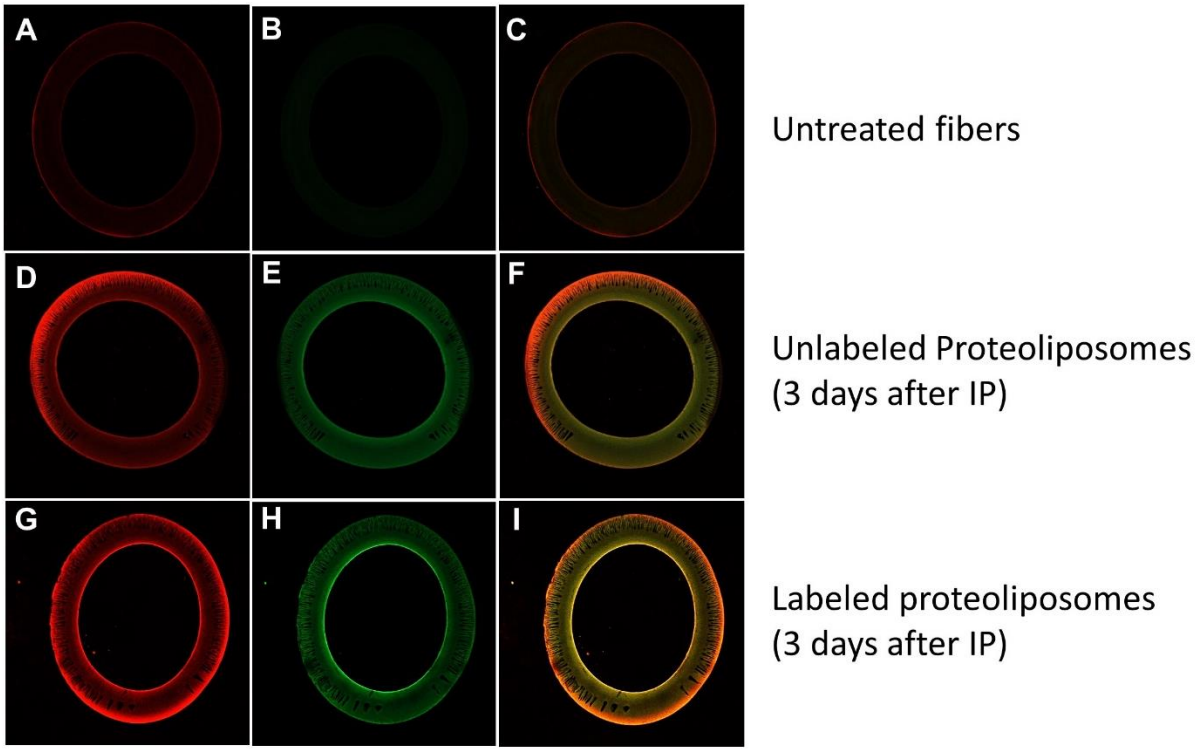

Supplementary Figure 3. Fluorescence of untreated hollow fibers and proteoliposomes (labeled and unlabeled) three days after IP. Representative slices of hollow fiber corresponding to (A-B) raw (untreated) fiber, (D-F) unlabeled AqpZ proteoliposomes and (G-I) labeled AqpZ proteoliposomes. Confocal microscope conditions as indicated in Materials and Methods section 2.10. All images were processed in identical conditions. The first and second columns represent the "red" and "green" channels (see section 2.10) and the third is an overlay.

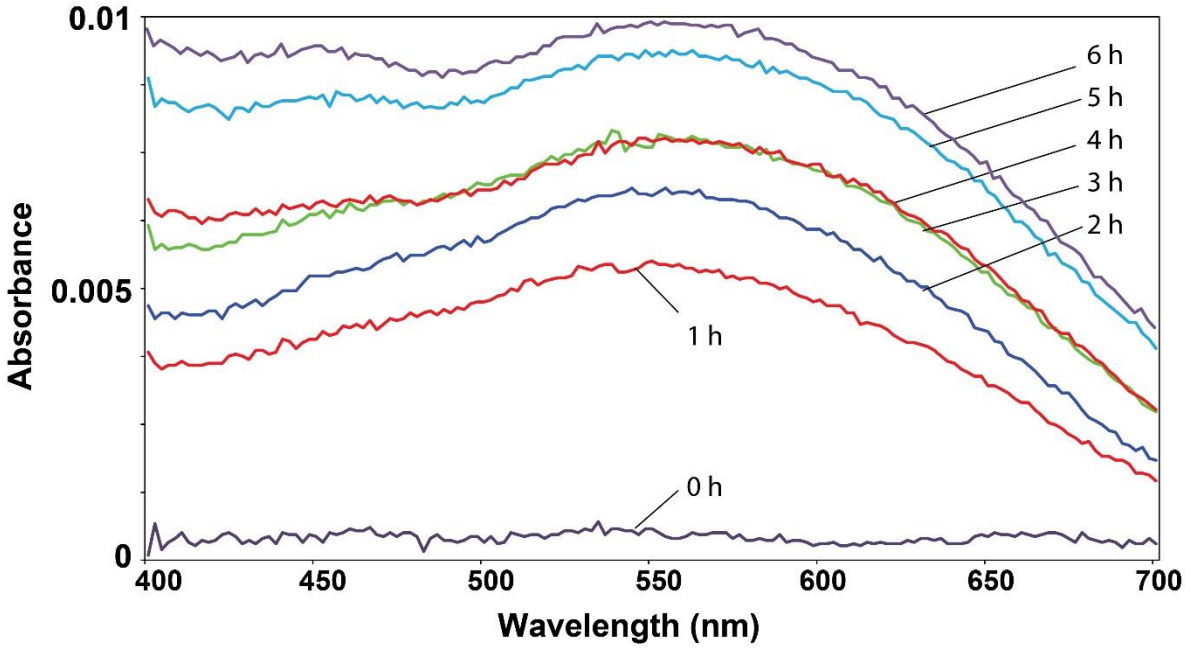

Supplementary Figure 4. Absorbance of a 1.2% MPD solution exposed to air. Spectra were obtained in 1 h intervals for 6 h (see labels). Despite absorbance increasing with time, the compound formed was not fluorescent after excitation over the whole range in the visible region (not shown).

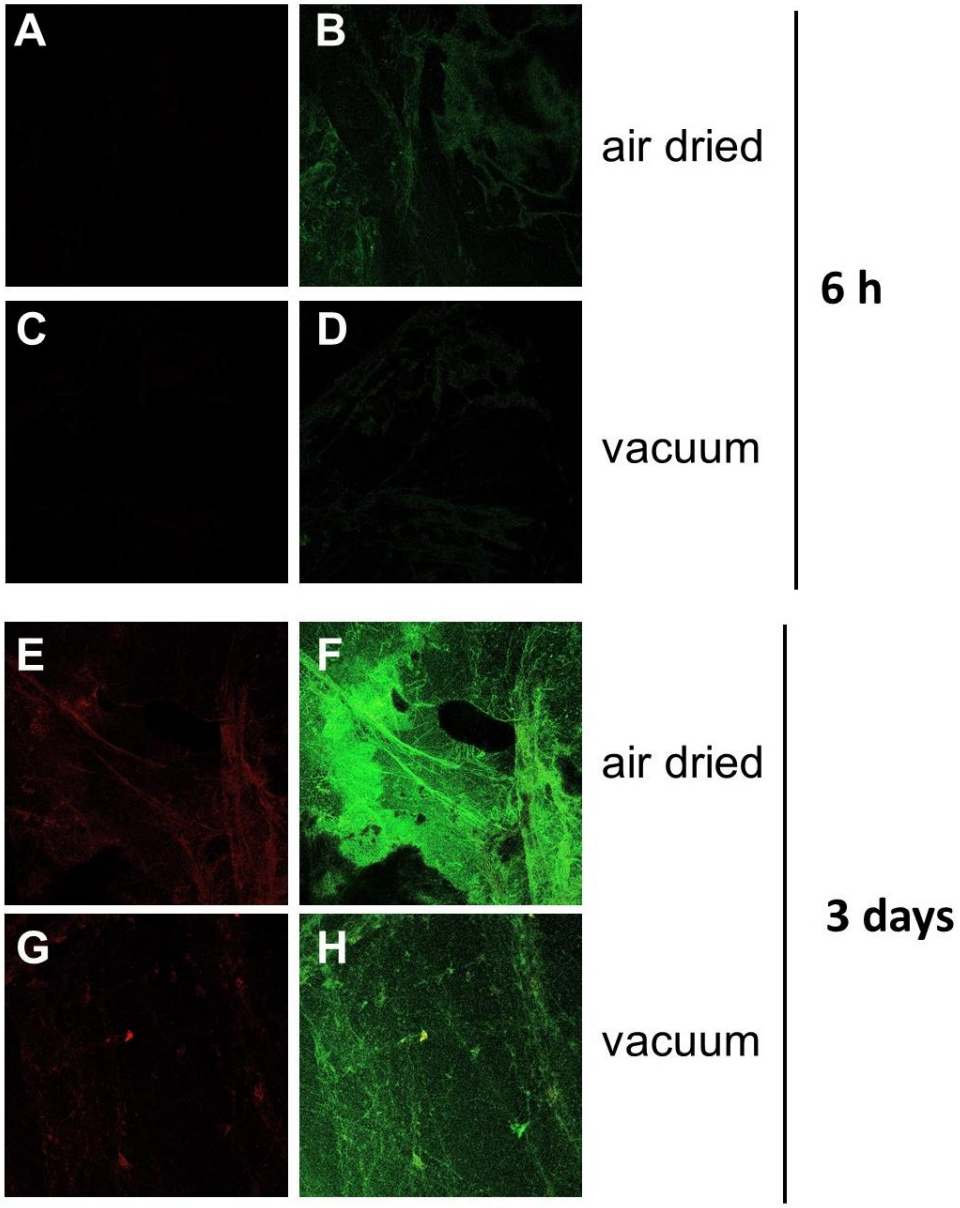

Supplementary Figure 5. Fluorescence of dry interfacial polymer obtained from a solution. The polymer was formed by mixing equal volumes of 1.2 % MPD in water and 0.15 % TMC in cyclohexane (see Materials and Methods section 2.11). (A-D) polymer formed observed after 6 h after IP formation, either dried in air (A-B) or dried under vacuum (C-D); (E-H) same as above but observed three days after IP formation, either dried in air (E-F) or under vacuum (G-H). First and second column represent the red and green channel, respectively.

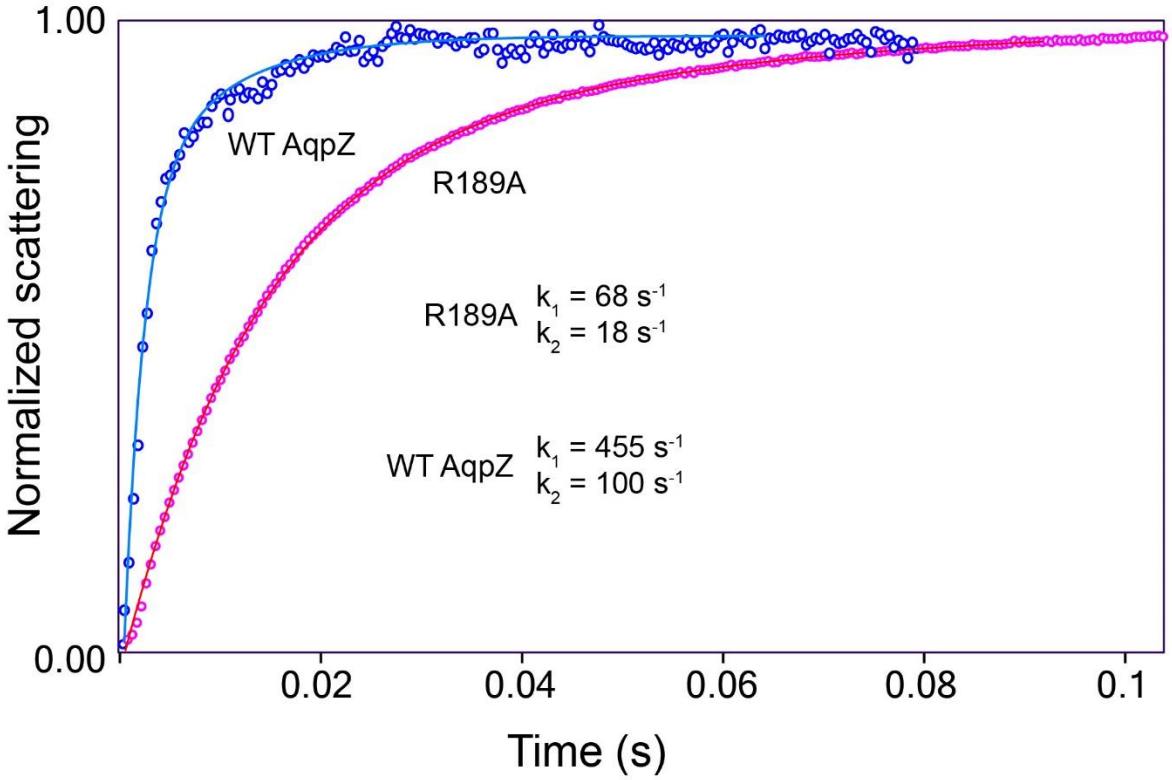

Supplementary Figure 6. Permeability of wild type (WT) AqpZ and AqpZ R189A mutant. Conditions of the experiment are described in Materials and Methods section 2.4. Circles are data points whereas the line is a fitted double exponential function with rate constants k_1 and k_2 indicated. Temperature was 15 °C. The fast component was used to calculate P_f and p_f [29]. The unitary permeability p_f of wild type AqpZ was 4.37 (± 1.3) x 10^{-14} $cm^3 \cdot s^{-1}$ (n = 4) whereas the R189A mutant p_f was 0.87 (± 0.3) x 10^{-14} $cm^3 \cdot s^{-1}$ (n = 2). The wild type AqpZ permeability is of the same order of magnitude as those reported previously, e.g., Borgnia et al. (10 x 10^{-14}) [29], Horner et al. (17 x 10^{-14}) [33], Schmidt and Sturgis (11 x 10^{-14})[34] and Zhao et al (3.2 x 10^{-14}) [18].

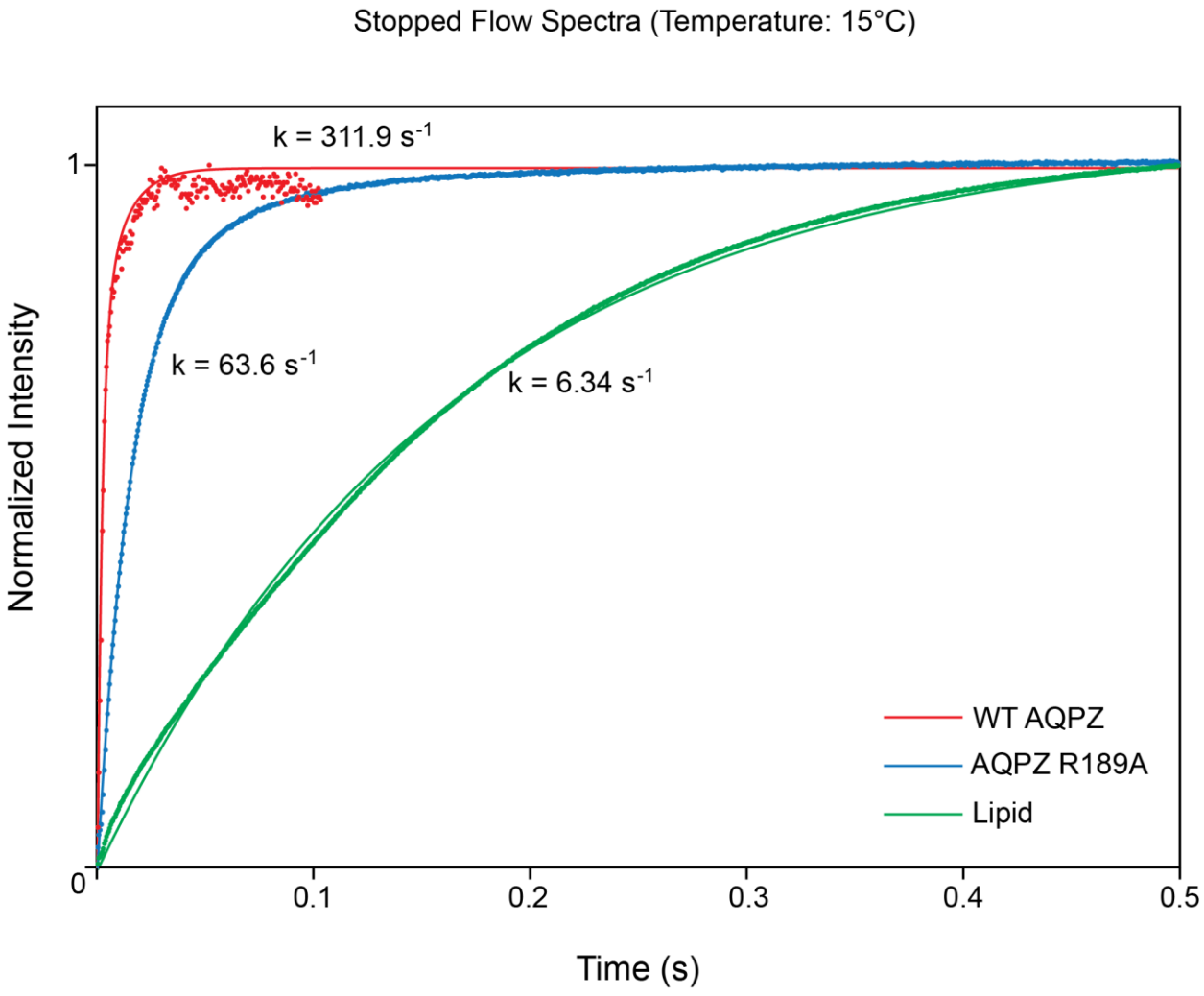

Supplementary Figure 7. Comparison of rate constants obtained for wild type (WT) AqpZ, AqpZ R189A mutant and lipid-only liposomes. Conditions of the experiment are described in Materials and Methods section 2.4. The line is a fitted single exponential function with rate constants indicated at temperature of 15 °C. The permeability of R189A membranes is about one order of mgnitude higher than that of lipid-only liposomes.

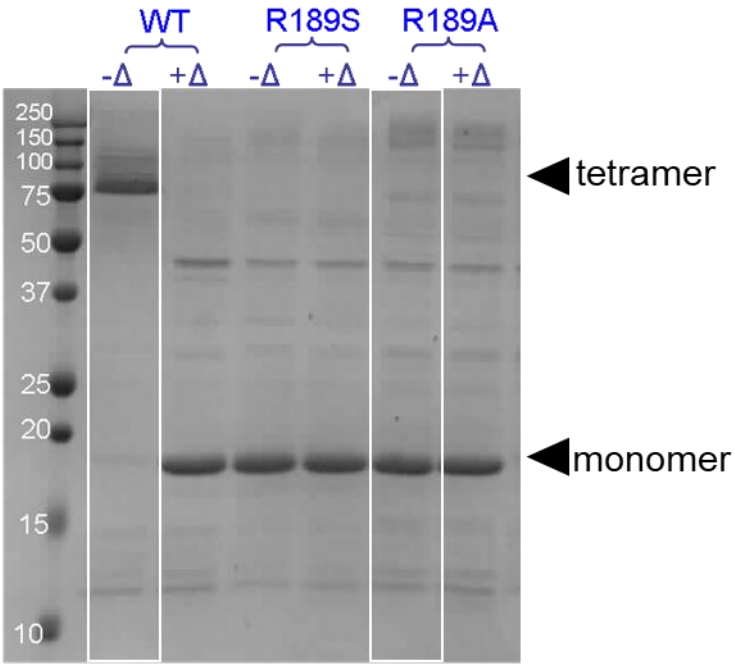

Supplementary Figure 8. Comparison of stability of WT AqpZ and mutants at position R189. SDS-PAGE of eluted fraction from IMAC column at room temperature (-Δ) or after heating at 70 °C for 5 min (-Δ). The position of tetramers and monomers is indicated with an arrow. WT AqpZ forms tetramers at room temperature, but mutant R189A forms monomers.

Equation 1. Liposomes per μm^2 required to cover uniformly a surface with a single layer of intact non-overlapping liposomes of 150 diameter gives ~44 liposomes/ μm^2 [36].

$$N = \frac{1000\ nm \times 1000\ nm}{2\ R \times 2\ R} = \frac{1000\ nm \times 1000\ nm}{150 \times 150} = 44\ vesicles \quad (1)$$

Equation 2. Formula to obtain the permeability (A) of the membranes as proposed in [36] from the Pf value obtained in the stopped-flow experiment, where A is the permeability ($\mu m\ s^{-1}\ bar^{-1}$), Vw is the volume of one mole of water, R is the gas constant and T is the temperature (K).

$$A = \frac{P_f \times V_w}{R \times T} \quad (2)$$

113

114

115

Supplementary File.

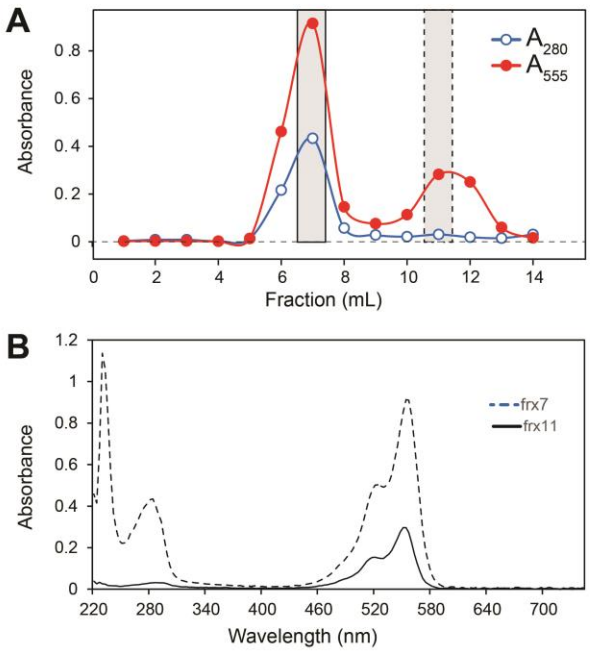

Supplementary Figure 1. Labeling of AqpZ. (A) Size exclusion chromatography of AqpZ after incubation with Alexa-555 dye, monitored at 280 and 555 nm; (B) UV-Vis spectra of fractions 7 (labeled AqpZ) and 11 (free dye) corresponding to the two peaks in (A). Both labeled AqpZ and free dye absorb at 555 nm (fractions 7 and 11), but only AqpZ absorbs strongly at 280 nm (fraction 7).

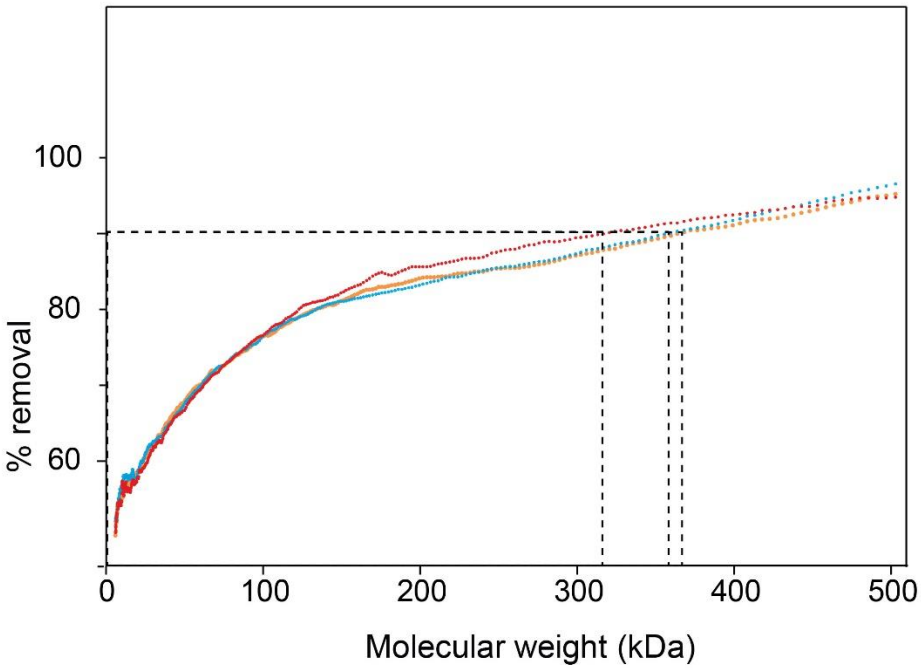

Supplementary Figure 2. Molecular weight cut-off (MWCO) of hollow fiber support. Dextran solutions with molecular weights ranging from 6-500 k were evaluated after examining composition of feed and draw. The MWCO was taken as the molecular weight of dextran rejected >90% (see dotted line).

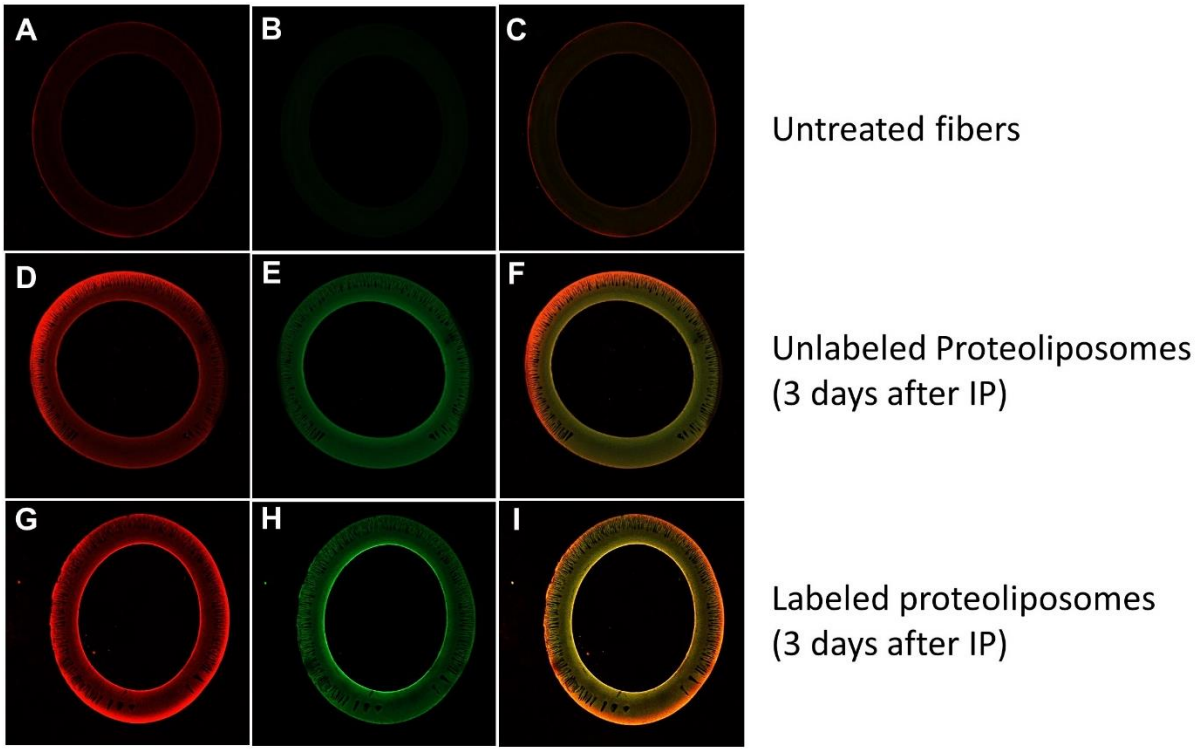

Supplementary Figure 3. Fluorescence of untreated hollow fibers and proteoliposomes (labeled and unlabeled) three days after IP. Representative slices of hollow fiber corresponding to (A-B) raw (untreated) fiber, (D-F) unlabeled AqpZ proteoliposomes and (G-I) labeled AqpZ proteoliposomes. Confocal microscope conditions as indicated in Materials and Methods section 2.10. All images were processed in identical conditions. The first and second columns represent the "red" and "green" channels (see section 2.10) and the third is an overlay.

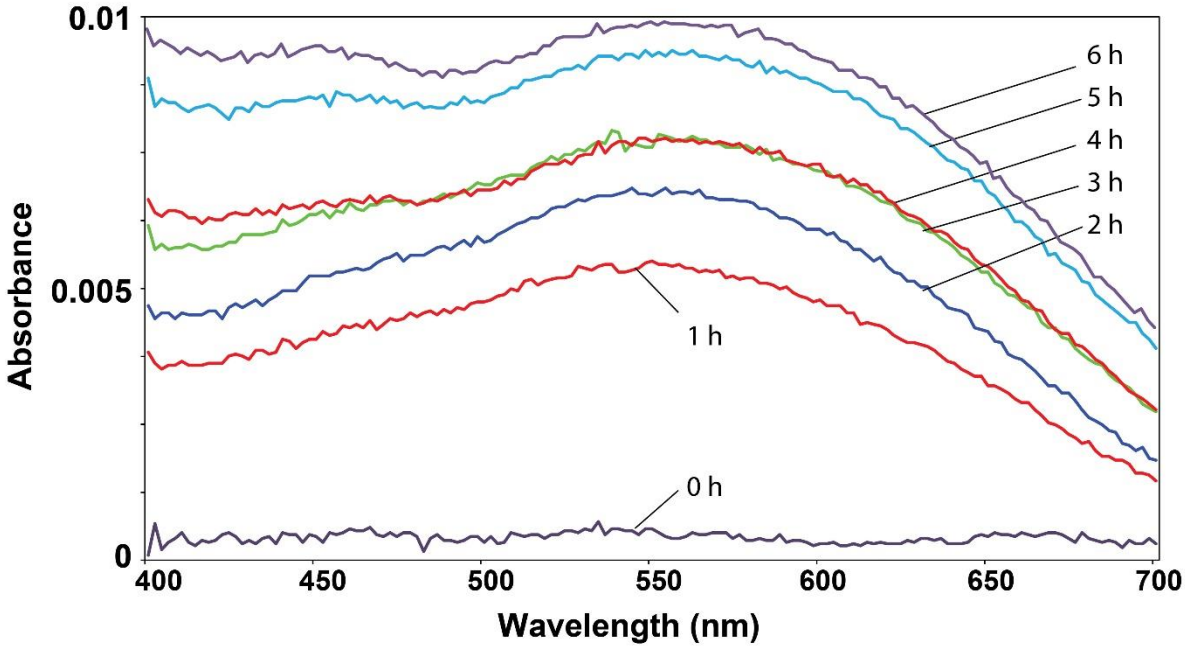

Supplementary Figure 4. Absorbance of a 1.2% MPD solution exposed to air. Spectra were obtained in 1 h intervals for 6 h (see labels). Despite absorbance increasing with time, the compound formed was not fluorescent after excitation over the whole range in the visible region (not shown).

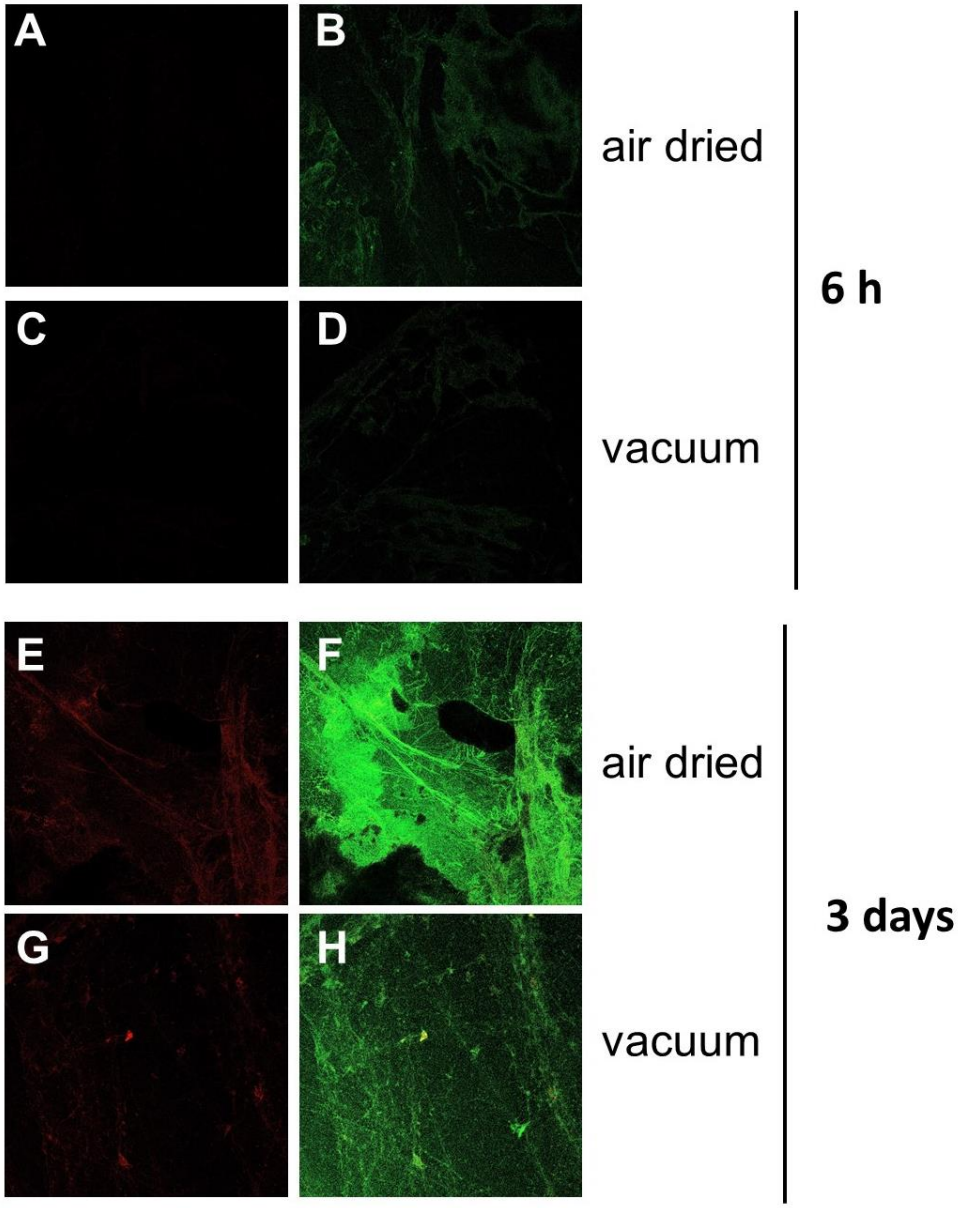

Supplementary Figure 5. Fluorescence of dry interfacial polymer obtained from a solution. The polymer was formed by mixing equal volumes of 1.2 % MPD in water and 0.15 % TMC in cyclohexane (see Materials and Methods section 2.11). (A-D) polymer formed observed after 6 h after IP formation, either dried in air (A-B) or dried under vacuum (C-D); (E-H) same as above but observed three days after IP formation, either dried in air (E-F) or under vacuum (G-H). First and second column represent the red and green channel, respectively.

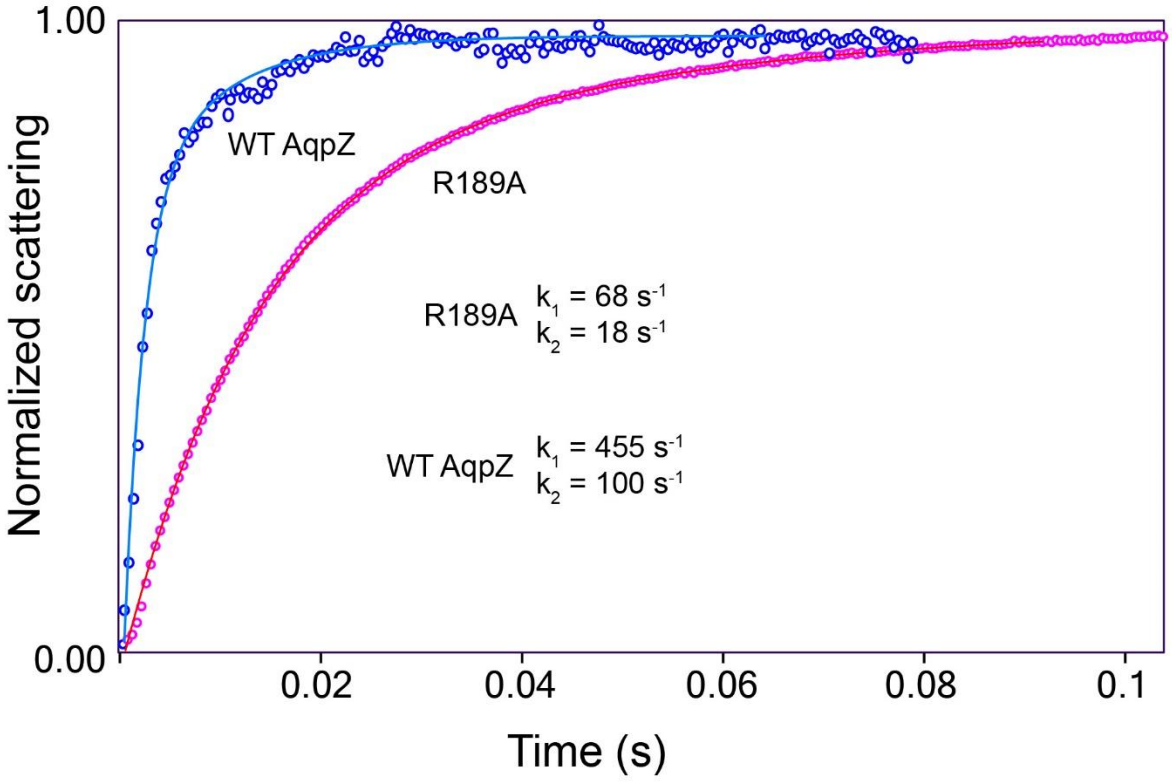

Supplementary Figure 6. Permeability of wild type (WT) AqpZ and AqpZ R189A mutant. Conditions of the experiment are described in Materials and Methods section 2.4. Circles are data points whereas the line is a fitted double exponential function with rate constants k_1 and k_2 indicated. Temperature was 15 °C. The fast component was used to calculate P_f and p_f [29]. The unitary permeability p_f of wild type AqpZ was 4.37 (± 1.3) x 10^{-14} $cm^3 \cdot s^{-1}$ (n = 4) whereas the R189A mutant p_f was 0.87 (± 0.3) x 10^{-14} $cm^3 \cdot s^{-1}$ (n = 2). The wild type AqpZ permeability is of the same order of magnitude as those reported previously, e.g., Borgnia et al. (10 x 10^{-14}) [29], Horner et al. (17 x 10^{-14}) [33], Schmidt and Sturgis (11 x 10^{-14})[34] and Zhao et al (3.2 x 10^{-14}) [18].

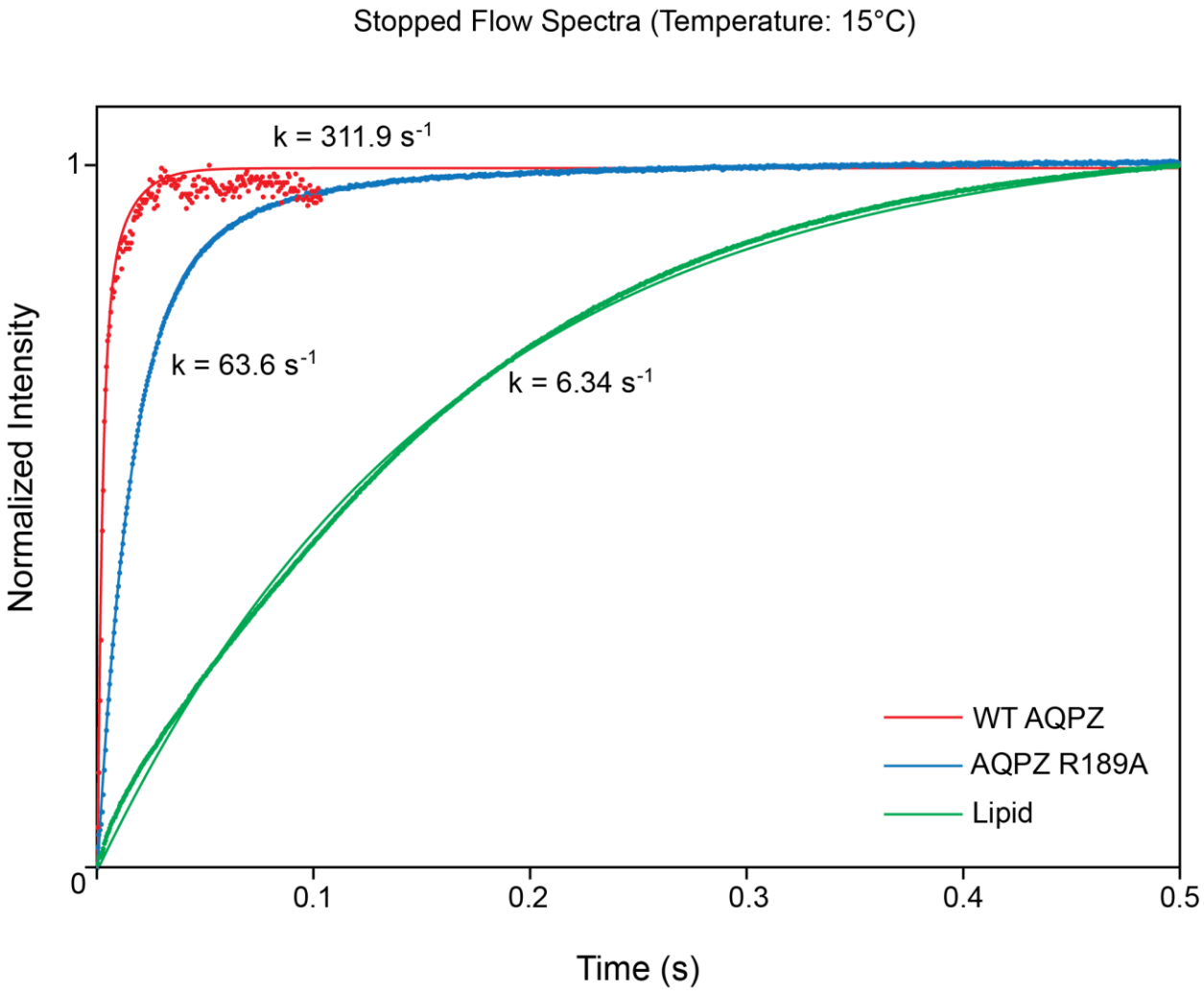

Supplementary Figure 7. Comparison of rate constants obtained for wild type (WT) AqpZ, AqpZ R189A mutant and lipid-only liposomes. Conditions of the experiment are described in Materials and Methods section 2.4. The line is a fitted single exponential function with rate constants indicated at temperature of 15 °C. The permeability of R189A membranes is about one order of mgnitude higher than that of lipid-only liposomes.

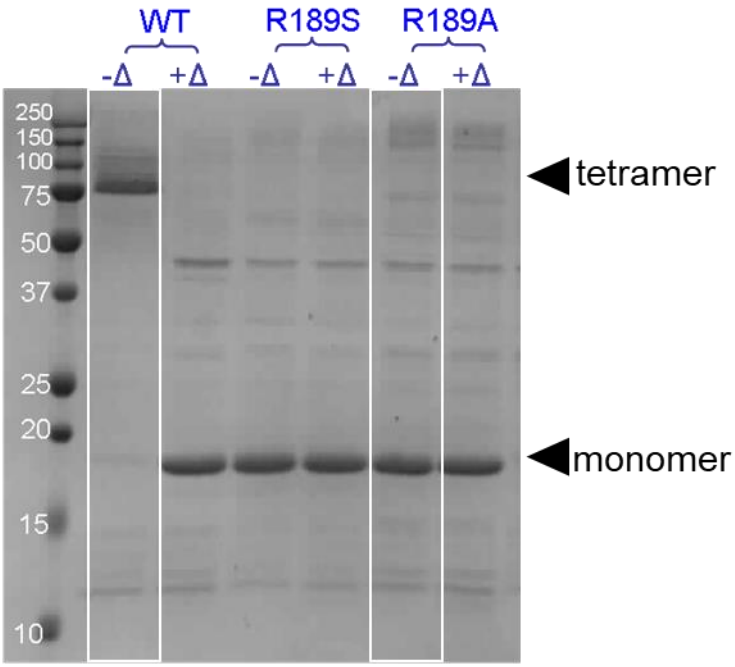

Supplementary Figure 8. Comparison of stability of WT AqpZ and mutants at position R189. SDS-PAGE of eluted fraction from IMAC column at room temperature (-Δ) or after heating at 70 °C for 5 min (-Δ). The position of tetramers and monomers is indicated with an arrow. WT AqpZ forms tetramers at room temperature, but mutant R189A forms monomers.

Equation 1. Liposomes per μm^2 required to cover uniformly a surface with a single layer of intact non-overlapping liposomes of 150 diameter gives ~44 liposomes/ μm^2 [36].

$$N = \frac{1000\ nm \times 1000\ nm}{2\ R \times 2\ R} = \frac{1000\ nm \times 1000\ nm}{150 \times 150} = 44\ vesicles \quad (1)$$

Equation 2. Formula to obtain the permeability (A) of the membranes as proposed in [36] from the Pf value obtained in the stopped-flow experiment, where A is the permeability ($\mu m\ s^{-1}\ bar^{-1}$), Vw is the volume of one mole of water, R is the gas constant and T is the temperature (K).

$$A = \frac{P_f \times V_w}{R \times T} \quad (2)$$

113

114

115